Magnetic Excitations of Finite Systems: Edge Effects on Spin Waves

by

Seamus Beairsto
B.Sc., St. Francis Xavier University, 2017

A Thesis Submitted in Partial Fulfillment of the
Requirements for the Degree of

MASTER OF SCIENCE

in the Department of Physics and Astronomy

Magnetic Excitations of Finite Systems: Edge Effects on Spin Waves

by

Seamus Beairsto
B.Sc., St. Francis Xavier University, 2017

Supervisory Committee

Dr. R. de Sousa, Supervisor
(Department of Physics and Astronomy)

Dr. B. Choi, Departmental Member
(Department of Physics and Astronomy)

Supervisory Committee

Dr. R. de Sousa, Supervisor
(Department of Physics and Astronomy)

Dr. B. Choi, Departmental Member
(Department of Physics and Astronomy)

ABSTRACT

This thesis explores finite-size effects on the spin wave excitations of one-dimensional ferromagnetic and antiferromagnetic systems. Specifically, it presents a theoretical study of the scattering function, the physical observable in inelastic neutron and photon scattering experiments, under the influence of extra magnetic anisotropy energy localized at the system's boundaries.The method for calculating spin wave scattering functions in bulk is adapted to the finite system case, enabling explicit numerical calculations with edge effects. Our results show a significant broadening of the scattering peaks of low energy spin waves in ferromagnetic and antiferromagnetic systems. We show that broadening is due to the emergence of spin excitations localized at the edge of the system, the so called edge modes.

Contents

List of Figures

Acknowledgements

I would like to thank:

my friends, family, and beautiful British Columbia, for supporting me in the low moments.

Dr. Rogério de Sousa, for mentoring, support, encouragement, and patience.

If we live our lives looking for the excitement and exhilaration that change can bring, we will be much happier than when we are eventually forced to accept it anyways.
Daniel Willey

Dedication

To Shadowfax, who is swift and sure.

Chapter 1

Introduction

1.1 Overview of the Thesis

In this work, we explore the effects of finite size and edge anisotropy on the scattering function of 1D ferromagnetic (FM) and antiferromagnetic (AFM) systems. In particular, we examine the spin wave scattering function that gives a description of inelastic scattering experiments using neutrons and photons. Through the study of these finite 1D systems, we gain valuable insights into the behaviour of spin waves (SWs, also known as magnons) and the interpretation of inelastic neutron scattering (INS) [1] and optical Raman scattering [2] experiments of magnetic nanoparticles. SWs provide a tool through which physicists can probe the physical properties of magnetic nanoparticles, which differ significantly from their bulk parents [3, 4, 5]. Understanding the properties of nanoscale magnetic systems is crucial to the fields of spintronics, magnetic memory storage, biomedical research, and more [6, 7, 8].

Our approach is an adaptation to finite systems, of the framework for evaluating the INS scattering function outlined by Fishman *et. Al.* [1]. The scattering function's evaluation requires taking the space and time Fourier transform of the eigenvectors of the equations of motion (EOM) of the spins. For systems with lattice translational symmetry, Fourier transformation diagonalizes the EOM of the spins. For finite systems without periodic boundary conditions, the full lattice translation symmetry is not present, and Fourier transformation is no longer sufficient to find the spin wave spectra. Therefore, we employ numerical diagonalization of the EOM, the eigensystem of which we use in the evaluation of the scattering function.

While previous studies have explored the INS scattering function of nanoparticle

systems through various means [9, 10], our approach allows for the determination of the yet unknown effects of edge anisotropy on INS scattering in finite systems. The development of our approach to evaluating the scattering function required unique adaptations of the framework outlined by Fishman.

Our results show the rise of acoustic and optical SW edge modes in both FM and AFM cases. FM edge modes appear in the presence of extra magnetic anisotropy at the edges of the system (edge anisotropy). When the extra anisotropy is easy plane (EP), the edge mode is *acoustic* (low frequency). If instead the anisotropy is easy axis (EA), the edge mode is *optical* (high-frequency). These edge modes have been previously theorized in the study of FM thin films [11, 12, 13]; however, their effect on INS and the spin wave scattering function has not been explored.

The phenomenology of edge modes for AFM systems is much less explored in the literature. Here we show that the nature of the edge mode is quite different in AFM systems. An edge mode does appear in AFMs even without edge anisotropy, so long that the system possesses *bulk* EA magnetic anisotropy (equal for all spins) and open boundaries. Similar to the FM case, an optical edge mode arises in the presence of large EA edge anisotropy, while EP edge anisotropy lowers the energy of the acoustic edge mode.

This thesis will follow the chapters outlined below.

Chapter 1 motivates the problem of magnetic excitations in finite systems and gives a basic introduction to spin waves in FM and AFM systems.

Chapter 2 describes our theoretical method to evaluate spin wave spectra and scattering function in finite systems.

Chapter 3 describes our results for FM systems.

Chapter 4 describes our results for AFM systems.

Chapter 5 discusses our results in the context of the literature, provides conclusions and avenues for future work.

1.2 Motivation

Recent studies suggest that edge anisotropy plays a significant role in the behaviour of magnetic nanoparticle systems. Of particular interest to us are recent works by Ian Aupiais, Marc Allen, and others [2, 14], demonstrating the effects of edge anisotropy on Bismuth Ferrite ($BiFeO_3$) nanoparticles. The Raman spectra in figure 1.2 shows the behaviour of optical Raman scattering of SWs in $BiFeO_3$ nanoparticles as particle size decreases; however, the physical interpretation of what is happening is unclear. Work by Mark Allen suggests that magnetic anisotropy at the surface of the nanoparticles causes inhomogeneous broadening of the spin wave excitations, leading to vanishing of optical Raman scattering peaks. While a 3D $BiFeO_3$ nanoparticle is vastly different from a 1D FM/AFM chain ($BiFeO_3$ has AFM cycloidal ordering [15]), we hope that we can shed light on the effects through investigation of a simple model of edge anisotropy on the scattering of SWs in finite systems. New understanding achieved in this work can then be applied to the problem of scattering in $BiFeO_3$ nanostructures, as well as other materials.

Additional motivation for studying the nature of the edge mode in finite 1D systems is that they provide the basic theoretical tool to describe surface spin wave modes in thin films. The spin dynamics of thin films can be described by a 1D spin chain perpendicular to the film's plane. In that case surface anisotropy becomes edge anisotropy for the 1D chain [11]. The edge mode becomes a surface mode in the thin film system, as described in figure 1.1.

1.3 Microscopic Origin of Magnetism

We start our story with a basic introduction to the microscopic mechanisms that give rise to magnetism. Spontaneous magnetic ordering in materials arises from the interaction of the constituent atoms, which themselves have a magnetic moment. This magnetic moment has two contributing factors, the orbital angular momentum of the electron orbiting the atom, as well as the intrinsic "spin" of the electron. Interaction between the spin of electrons in adjacent atoms is what leads to magnetic ordering.

Many microscopic mechanisms contribute to the exchange interaction between spins [16]. The Coulomb exchange mechanism (arising from the Pauli exchange integral) contributes to $J > 0$ and therefore favours ferromagnetism. It occurs be-

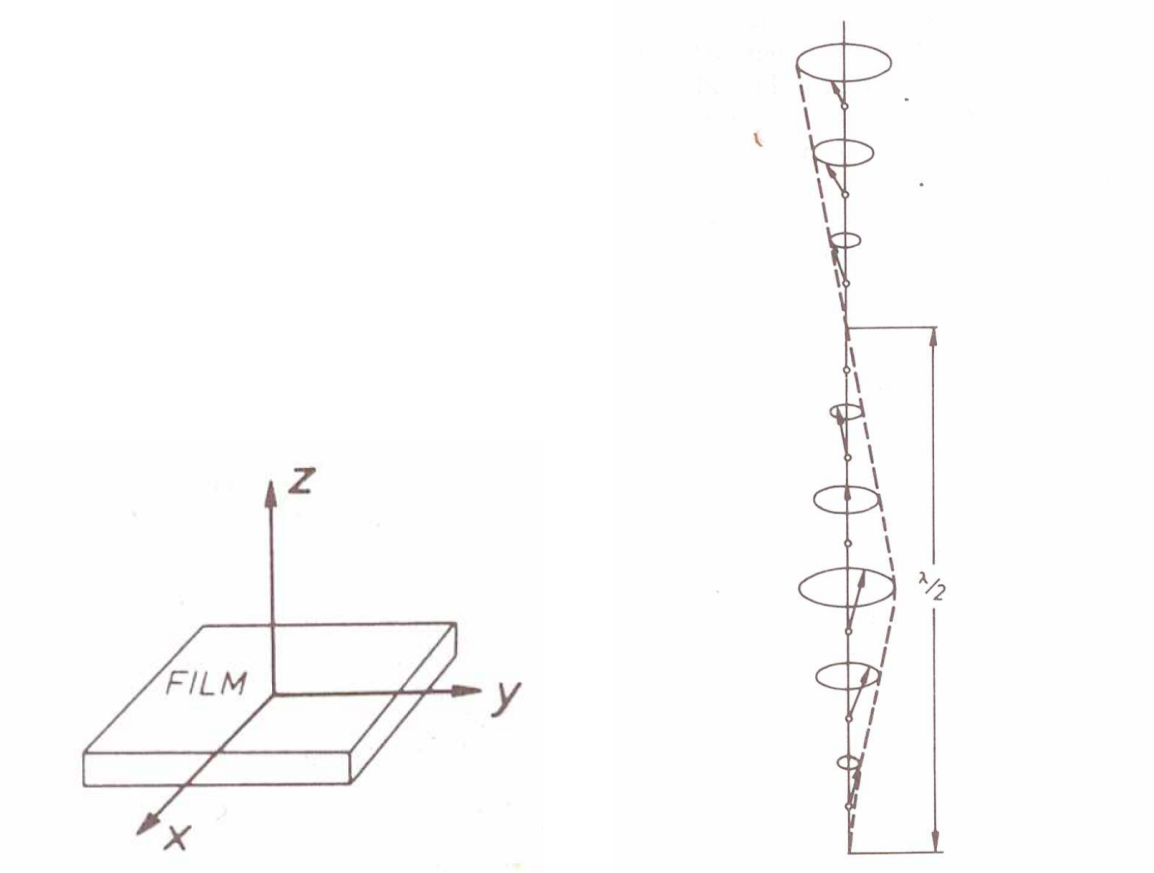

(a) (b)

Figure 1.1: Modelling of FM thin film as 1D spin chain (a) shows the thin film model, (b) shows the form of spin waves along the z-axis, modelled by a 1D spin chain [11].

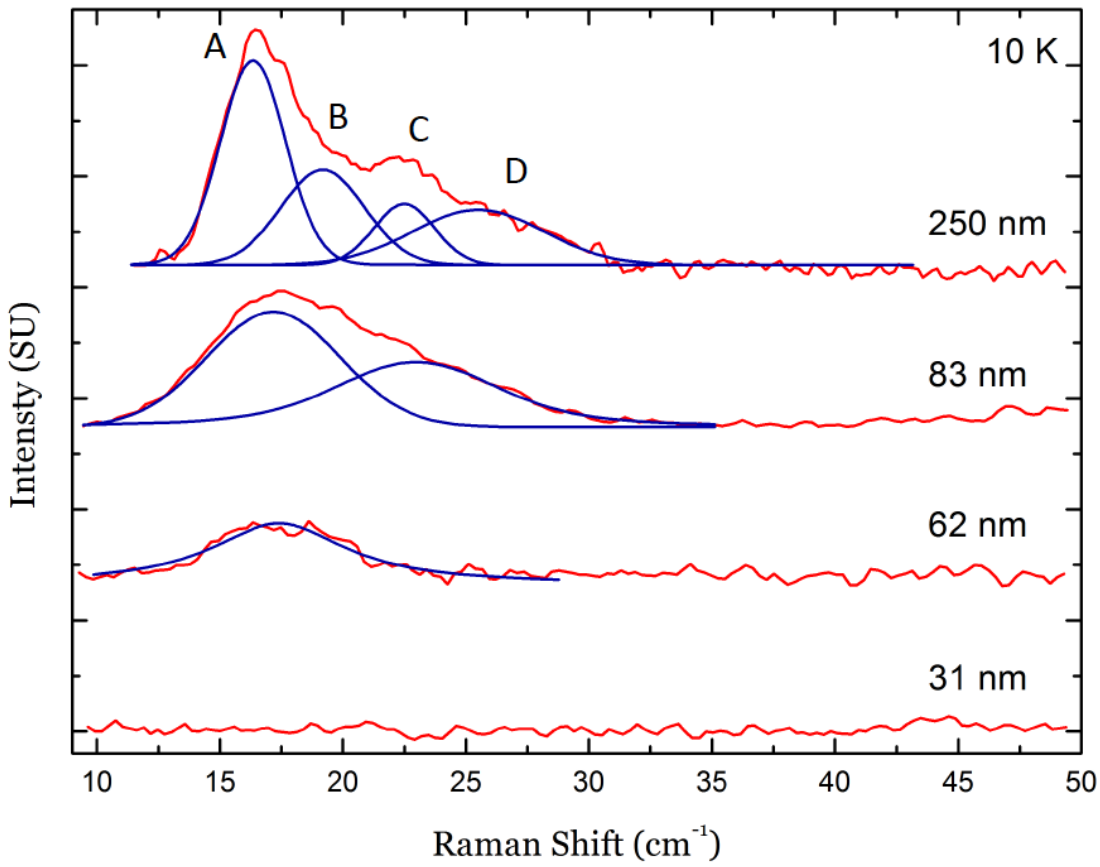

Figure 1.2: Raman scattering of BFO nanoparticles. We see the vanishing of SW peaks as particle size decreases, the explanation of which is yet unclear. [2]

cause antiparallel spins (two-electron singlet states) have orbital wavefunction that is symmetric under particle interchange, whereas parallel spins (two-electron triplets) necessarily have antisymmetric orbital wavefunctions. This results in a difference in the spacial wave function of the system, which due Coulomb repulsion, favours the parallel alignment of spins, because for antisymmetric orbitals the probability of electrons being on top of each other is zero. When the majority of spins in a system are aligned, the system will exhibit a spontaneous net magnetization, or ferromagnetism.

The direct exchange mechanism has the opposite sign of Coulomb exchange, i.e. it contributes to $J < 0$ (antiferromagnetism). Direct exchange occurs due to virtual hopping of electrons from one magnetic ion to the other. The Pauli exclusion principle requires that the spins of electrons occupying the same orbital are in a singlet state. As a result, virtual hopping is only allowed when the spins of neighbouring ions are antiparallel. As a result, direct exchange lowers the energy of singlet states in comparison to triplet states, contributing to $J < 0$.

The superexchange mechanism occurs due to virtual hopping of electrons from magnetic ions into an atom (usually oxygen) located in between them. Similar to direct exchange, superexchange always contributes to $J < 0$. A good example of this is in magnesium-oxide, where ionic bonding leads to linear chains of Mn^{2+} and O^{2-} ions running through the crystal. Along the chain direction the O^{2-} has a full p-orbital oriented along Mn-O-Mn. The Mn^{2+} ions have half-filled ($3d^5$) d-orbitals with parallel spins within each Mn^{2+}. It is energetically favourable to have covalent bonding between ions, and since the oxygen's p-orbital is full, it shares its electrons with the d-orbitals. The p-orbital shares an up-spin with one Mn^{2+} ion and a down-spin with the other. As the d-orbitals are half-full, the donated spin must anti-align with the other five spins in the orbital. The final result of this interaction is to have antiparallel alignment of the spins on either side of the O^{2-} ion favoured. This is the dominant interaction in some magnetic oxides. The result of antiparallel alignment of the spins is that while the crystal has spontaneous magnetic ordering, the magnetic moments of the spins cancel each other out, and the system has no net magnetic moment. This is referred to as antiferromagnetism.

1.4 Spin Waves

The goal of this study is to elucidate the properties of elementary magnetic excitations under a particular set of constraints. It, therefore, seems appropriate have a discussion of the general nature of magnetic excitations.

1.4.1 FM Spin Waves

We begin our journey with a one-dimensional insulating ferromagnet, which is described via the ferromagnetic Heisenberg Hamiltonian,

$$\hat{\mathcal{H}} = -J \sum_i \hat{\boldsymbol{S}}_i \cdot \hat{\boldsymbol{S}}_{i+1}. \tag{1.1}$$

Here J is the exchange constant, which must be positive to promote ferromagnetic ordering, i is the spin site index, and $\hat{\boldsymbol{S}}_i$ is the spin operator at site i given by $\hat{\boldsymbol{S}} = [\hat{S}_i^x, \hat{S}_i^y, \hat{S}_i^z]$. The ground state of this system has all the spins aligned along a single axis $\boldsymbol{\gamma}$ which we will take to be in the $\hat{z}$ direction without loss of generality.

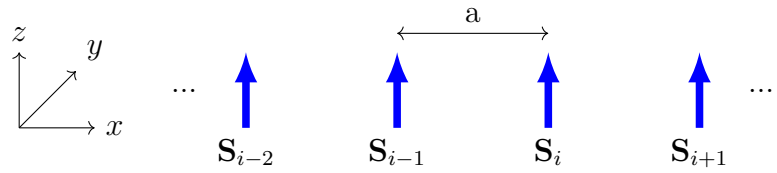

Excitations to this state take the form of a deviation of one of the spins from the z-axis. When this occurs, the rest of the spins in the chain adjust in a wave-like manner, thereby lowering the excitation's energy. Finding the equations of motion of the spins in these elementary excitations, or spin waves (SW), is not trivial, as the spin operators do not commute. In this work, we map our spin operators to boson creation and annihilation operators via the Holstein-Primakoff (HP) transformation [17]. We spare the details of this transformation for now, as we will go into it at great lengths when the time comes. Through the HP transformation, it is possible to express the magnetic Hamiltonian as

$$\hat{\mathcal{H}}_2 = \sum_q \omega_q \hat{a}_q^\dagger \hat{a}_q = \sum_q 2JS(1 - \cos(qa)) \hat{a}_q^\dagger \hat{a}_q, \tag{1.2}$$

where $\hat{a}_q^\dagger$ and $\hat{a}_q$ are the creation and annihilation operators for a boson excitation with the quantum number q which sums over the first Brillouin zone. These excitations correspond to the energy eigenstates of the system, with energy $\omega_q = 2JS(1-\cos(qa))$,

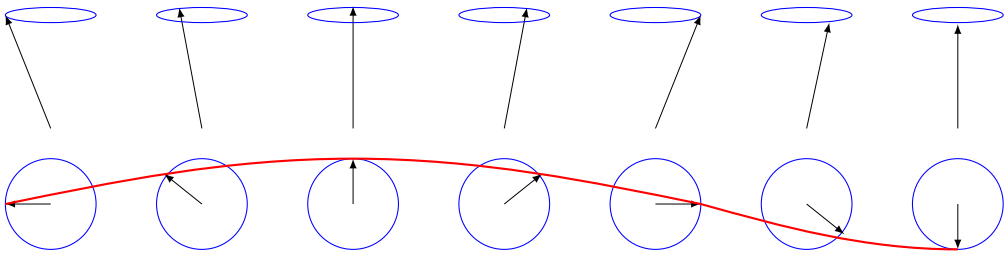

Figure 1.3: Side and top view of spins in a SW

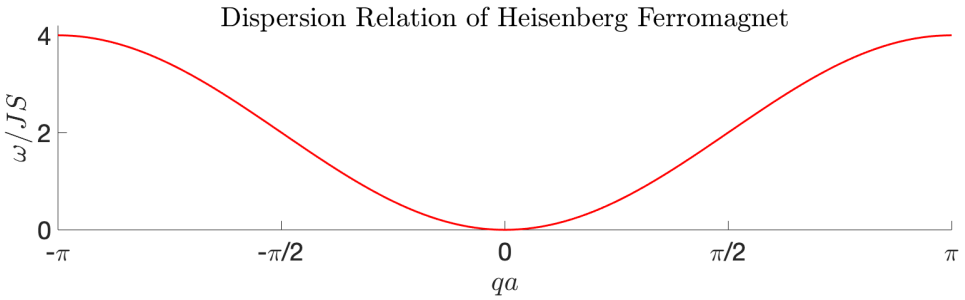

Figure 1.4: Dispersion relation of one-dimensional Heisenberg ferromagnet, given by Eq. 1.2.

which is the SW dispersion. Here we have taken $\hbar = 1$ for simplicity. The quantum number q corresponds to the wavenumber of the plane wave solutions to the equations of motion. The semi-classical picture here has the spin at each site i precessing about the z-axis with a frequency ω_q; the spin at each site being out of phase with its neighbour by qa. The dispersion relation relates the frequency of the oscillation ω_q to the wavenumber q.

We can see here that for low q, $\omega_q \propto q^2$ for a FM, and, as $q \to 0$, we have $\omega_q \to 0$. The $q = 0$ mode corresponds to a uniform rotation of all the spins, called a Goldstone mode. The rotational symmetry of the Hamiltonian guarantees the existence of the Goldstone mode. We chose for the ground state to have the spins $\boldsymbol{S}_i^{(G)}$ align along the z-axis, but this choice was arbitrary. We could have equally chosen for $\boldsymbol{S}_i^{(G)}$ to lie along x or y or any other direction. The introduction of an external magnetic field or an anisotropy field destroys this rotational symmetry, forcing $\boldsymbol{S}_i^{(G)}$ to align along the direction of the external fields. The breaking of the rotational symmetry opens up a gap in ω, resulting in $\omega_{q=0} > 0$. The low energy excitations will be of particular interest to us in this study.

1.4.2 AFM Spin Waves

The second portion of our study investigates spin waves in the one-dimensional insulating antiferromagnet. We can interpret the Heisenberg antiferromagnet as two interlaced ferromagnetic sublattices, A and B, which anti-align with one another in the ground state. We again arbitrarily choose $\hat{\boldsymbol{z}}$ as the axis of alignment, without loss of generality.

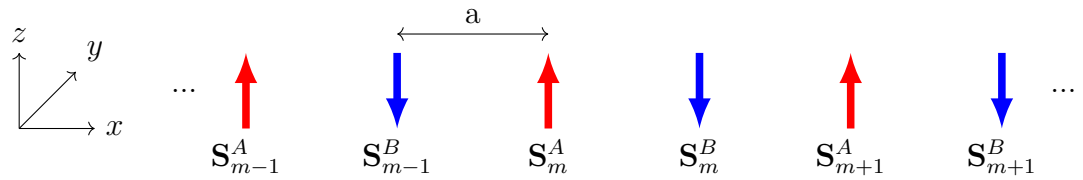

We describe he Heisenberg antiferromagnet via the Hamiltonian,

$$\hat{\mathcal{H}} = -J \sum_m \hat{\boldsymbol{S}}^A_m \cdot \hat{\boldsymbol{S}}^B_m - J \sum_m \hat{\boldsymbol{S}}^B_m \cdot \hat{\boldsymbol{S}}^A_{m+1}, \tag{1.3}$$

where $\hat{\boldsymbol{S}}^A$ is the spin operator for spins on lattice A, $\hat{\boldsymbol{S}}^B$ is the spin operator for spins on lattice B, and $J < 0$. The HP transformation is again applied in concert with a Fourier transform to diagonalize the equations of motion; however, an additional transformation, a Bogoliubov transformation, is required to decouple the SWs in lattices A and B. The result is

$$\hat{\mathcal{H}}_2 = \sum_q \omega^a_q \hat{a}^\dagger_q \hat{a}_q + \sum_q \omega^b_q \hat{b}^\dagger_q \hat{b}_q, = 2JS \sum_q |\sin(qa)| (\hat{a}^\dagger_q \hat{a}_q + \hat{b}^\dagger_q \hat{b}_q) \tag{1.4}$$

where q again sums over the first Brillouin zone, $\hat{a}_q$ is the creation operator for SW excitations on lattice A, and $\hat{b}^\dagger$ is the creation operator for SWs on lattice B. Each lattice has a dispersion relation; however, in the infinite case, the two lattices' dispersion relations are degenerate. Fig. 1.5 shows the resulting dispersion relation. We see here that for low q, $\omega \propto q$, again having $\omega \to 0$ when $q \to 0$.

Now that we provided the basic idea of what a SW is in the context of FM and AFM systems, we will describe the methods used to detect SWs.

1.5 Inelastic Neutron Scattering

Many experimental methods are useful in measuring and characterizing SWs; however, the nanoscale size of our systems will prove to be somewhat prohibitive in

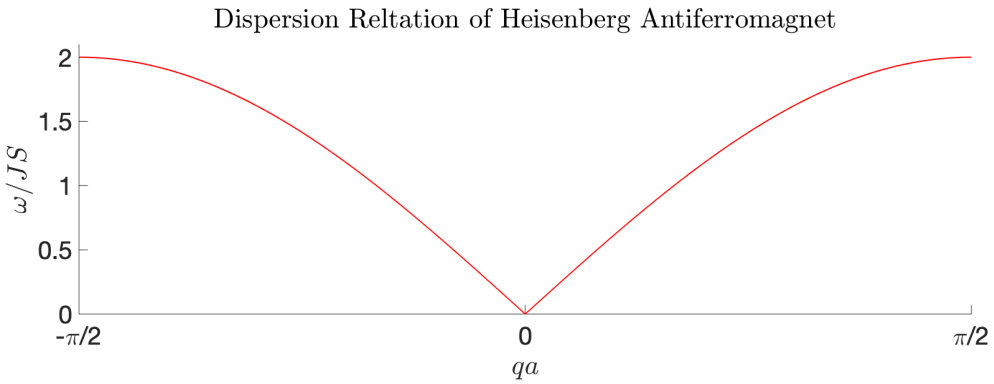

Figure 1.5: Dispersion relation of one-dimensional Heisenberg antiferromagnet, given by Eq. 1.4

selecting a particular method to model [1]. Recent studies focus on the use of INS and optical Raman spectroscopy in the study of SWs excitations in nanoparticles [9, 2, 18]. We will focus our attention on INS as its scattering function relies directly on the eigenstates of the SWs, whereas Raman scattering requires the additional treatment of the spin-orbit coupling [19].

Neutrons have no electric charge and are weakly interacting, which makes them ideal candidates for probing the inner structure and dynamics of condensed-matter systems. The wavelength of neutrons is on the length scale of interatomic spacings, which lends them to the study of material structures. At the same time, their energy is on the same order as thermal fluctuations in solids, which makes them ideal for studying lattice dynamics. Furthermore, the neutron spin couples to electronic spins in the system, allowing them to probe magnetic structures and SWs [20].

The neutron scattering process begins with the neutrons produced either via nuclear fission in a reactor or spallation at an accelerator. The neutrons are then cooled through collisions with a moderator until they reach thermal equilibrium. We refer to these as thermal neutrons. The neutrons are then passed through a monochromator crystal, selecting only a narrow band of wavelengths. We now have an incident beam of neutrons with linear momentum $\hbar\boldsymbol{k}_i$ and energy $\hbar\omega_i = (\hbar\boldsymbol{k}_i)^2/2m_n$, where m_n is the neutron mass. The neutrons then scatter through interactions with the nuclei and electronic spins of the sample. The momentum and energy of the scattered neutrons are then measured from which we can get information on the structure and spin dynamics of the system.

We let

$$\hbar\boldsymbol{\kappa} = \hbar(\boldsymbol{k}_i - \boldsymbol{k}_f) \tag{1.5}$$

and

$$\hbar\omega = \frac{\hbar^2}{2m_n}(\boldsymbol{k}_i^2 - \boldsymbol{k}_f^2) \tag{1.6}$$

be the momentum and energy transferred to the system by the incident neutrons.

The energy $\hbar\omega \neq 0$ imparted to the system via INS creates or destroys elementary excitations such as SWs. $\boldsymbol{\kappa}$ is related to the momentum transferred to the system;

however, the wave vector $\boldsymbol{q}$ associated with the excitation must lie within a single Brillouin zone (BZ). $\boldsymbol{q}$ is related to $\boldsymbol{\kappa}$ via $\boldsymbol{\kappa} = \boldsymbol{q} + \boldsymbol{\tau}$, where $\boldsymbol{\tau}$ is an allowed reciprocal lattice vector of the system. This relation holds if the periodicity of the magnetic structure matches that of the atomic structure, such as in the case of the FM studied previously. If the periodicities differ, as is the case in an antiferromagnetic (AFM) system, a magnetic ordering wave vector $\boldsymbol{Q}$ must be included. $\boldsymbol{\kappa}$ is then written as, $\boldsymbol{\kappa} = \boldsymbol{\tau} + \boldsymbol{Q} + \boldsymbol{q}'$, where $\boldsymbol{q}' = \boldsymbol{q} - \boldsymbol{Q}$ is the excitation wave vector. For example, in a monatomic one-dimensional FM chain, the allowed values of τ are $\tau = n\frac{2\pi}{a}$, where n is an integer, a is the interatomic lattice spacing, and we have assumed the chain extends along the $\boldsymbol{x}$ direction in real space. As the periodicity of the magnetic structure of a FM is the same as that of the lattice, Q=0, and we can see that $q' = q \in [-\frac{\pi}{a}, \frac{\pi}{a}]$, corresponding to the first BZ. In the case of an AFM we still have $\tau = n\frac{2\pi}{a}$, however, the periodicity of the magnetic structure is now half that of the lattice, and $Q = \pm\frac{\pi}{a}$. The resulting excitation wave vector is $q' = q - Q \in [-\frac{\pi}{2a}, \frac{\pi}{2a}]$. (Note, that from here on out we will refer to the excitation wave vectors as $\boldsymbol{q}$ and not $\boldsymbol{q}'$)

INS directly measures the scattering function $S_{\alpha,\beta}(\boldsymbol{q}, \omega)$, which is the space and time Fourier transform of the time-dependent spin-spin correlation function,

$$S_{\alpha\beta}(\boldsymbol{q}, \omega) = \frac{1}{2\pi N} \sum_{i,j} \int dt e^{-i\omega t} e^{-i\boldsymbol{q}\cdot(\boldsymbol{R}_i - \boldsymbol{R}_j)} \left\langle \hat{S}_i^{\alpha}(0) \hat{S}_j^{\beta}(t) \right\rangle_T . \tag{1.7}$$

The spin-spin correlation function evaluates how closely correlated the spin at site i at time t is with spin j at time t' (can also be represented as $t = 0$ and $t' = t$ as we are only concerned with elapsed time). Generally speaking the further apart the spins are in time and space, the less correlated they will be. The spin-spin correlation function provides complete information on the spin-spin interactions in the system. We delve into the details of Eqn. 1.7 in the following chapter; however, from this expression, we can see that each neutron scattered with momentum $\hbar\boldsymbol{\kappa}$ and energy $\hbar\omega$, directly measures a single Fourier component of the spin-spin correlation function. The scattering function $S_{\alpha,\beta}(\boldsymbol{q}, \omega)$ will form the focal point through which we will investigate the behaviour of SWs in our system.

Finally, we provide a brief discussion on the value of Eq. 1.7 as a *proxy* for optical Raman scattering experiments. The spin scattering function 1.7 at $q \approx \omega/c \approx 0$, where c is the speed of light, describes the spectral weight for inelastic spin exci-

tations that *can* occur due energy and momentum conservation in optical Raman scattering. By no means all excitations that satisfy energy and momentum conservation do occur, as there is an additional criteria related to spin-orbit coupling for light absorption/emission.

A proper description of optical Raman scattering would involve the convolution of Eq. 1.7 with a structure factor that depends on spin-orbit coupling [19]. However, it is quite hard to calculate such structure factor from microscopic theory and the usual approach is to rely on symmetry arguments. In summary, we can interpret $S_{\alpha,\beta}(q=0,w)$ as a proxy for the expected strength of Raman peaks for photons that loose or gain energy $\hbar\omega$, but we should keep in mind that not all peaks are expected to lead to inelastic photon resonances.

1.6 Magnetic Anisotropy

One of the primary restraints we are going to impose on our system is magnetic anisotropy. Magnetic anisotropy is the tendency of a system to resist magnetization in some directions more than others. Previous work has shown that surface anisotropy, in particular, plays a crucial role in the magnetic dynamics of finite systems [11, 21]. We aim to quantify the effects of surface anisotropy in the spin-dynamics of nanoscale systems within the microscopic theory framework.

There are two general microscopic mechanisms for magnetic anisotropy. The first one is magnetocrystalline anisotropy [4], which refers to the tendency of the magnetization to align along crystallographic axes. The origin of this effect is the spin-orbit coupling. When we apply an external magnetic field to the sample, the electron spins try to align with the field direction. Electron spins couple to electron orbitals; therefore, the orbitals also align along the direction of the external field. The orbitals are also strongly coupled to the lattice, and therefore attempts to rotate the spin axes are strongly resisted.

The second microscopic mechanism leading to magnetic anisotropy is the dipolar interaction between spins. The total dipolar energy can be written as a volume integral of the magnetic field squared over the region outside the magnet [22]. When written in this way, this is called magnetostatic energy. This contribution is large for

FMs because they produce a large field outside their boundaries, and is negligible to AFMs because their anti-aligned spins only produce a negligible field. For FMs this leads to often denoted shape anisotropy. For example, a FM shaped like an ellipsoid will have its spin orientation favoured along the long axis of the ellipsoid [4].

The preference for the magnetization to lie along an axis, with two preferential directions, 180° apart, is referred to as easy-axis (EA) anisotropy. In some cases, the magnetization of the system prefers to lie perpendicular to a particular crystal axis, we refer to this as easy-plane (EP) anisotropy. The impact of bulk anisotropy on the spin wave spectra is well known [23], so we focus our study on the impact of surface/edge anisotropy.

1.6.1 Surface Anisotropy

Initially proposed by Néel [24], the microscopic mechanism of surface anisotropy is magnetocrystalline anisotropy. Surface anisotropy occurs because the symmetry of a magnetic ion at the surface is lower than the symmetry of a bulk ion. As a result, the magnetocrystalline anisotropy of a surface ion is different than the one for an ion in the bulk [24]. Surface anisotropy can also be either EA or EP. The most common situation is that the axis points perpendicular to the surface, and the plane is the surface itself. We introduce magnetic anisotropy to our one-dimensional Hamiltonian as,

$$\hat{\mathcal{H}} = -\frac{1}{2}J\sum_{i}\hat{S}_i\cdot\hat{S}_{i+1} - K\sum_{i}(\hat{S}_i^z)^2 - K_s\left[(\hat{S}_1^z)^2 + (\hat{S}_N^z)^2\right], \tag{1.8}$$

where and K_s and K are the magnitudes of the surface and bulk anisotropy, respectively, and z is the easy-axis direction. For $K_s > 0$, the edge spins will be pinned along the z-axis, and for $K_s < 0$, the spins are unpinned provided that they lie in the plane perpendicular to z. In large systems with small surface to volume ratio, the K_s term is negligible compared to the bulk anisotropy K; however, it becomes important for some nanoscale systems [21], which brings us to our second constraint of interest, finite size.

1.7 Magnetic Nanoparticles

The second constraint we impose on our system – finite size – goes hand in hand with surface anisotropy. In nanoparticle systems, a significant proportion of the atoms lie on the surface, which causes their properties to differ significantly from the bulk materials. We wish to highlight several finite-size effects before moving forward as they motivate some of the focus areas in our work.

1.7.1 Superparamagnetism

Superparamagnetism is a result of the reduction of the magnetic anisotropy energy due to finite size [25]. The anisotropy energy of a magnetic system is roughly proportional to its volume. Therefore, for small enough volumes, it can be on the same order as the thermal energy k_BT, where k_B is the Boltzmann constant, and T is the temperature. The result is that the system may be subject to magnetic reversals along the easy axis due to thermal excitations; we refer to these reversals as superparamagnetic relaxation. The superparamagnetic relaxation time is given by,

$$\tau = \tau_0 e^{KV/k_BT}, \tag{1.9}$$

where K is the bulk magnetic anisotropy constant, V is the particle volume, and τ_0 is on the order $\tau_0 \approx 10^{-13}s - 10^{-9}s$ [26]. If the relaxation time is long relative to the temporal resolution of the measurement technique, the instantaneous magnetization of the sample will be measured. However, if the relaxation time is on the same order as the temporal resolution, the average magnetization will be measured. This effect is particularly detrimental to studies investigating the temperature dependence of magnetization of nanoparticles. We refer to the temperature at which the two time scales are on the same order as the superparamagnetic blocking temperature T_B. In this case, the system will appear to have a zero net magnetization in zero external field; however, it will be extremely susceptible to an external field, more so than a paramagnetic system, hence the term "superparamagnetic." The temporal resolution of INS is on the order of picoseconds, making it an ideal tool for the examination of systems in the superparamagnetic regime [26]. While we investigate the full spectra of excitations, our findings for low-lying excitations should be of particular interest to those studying the temperature dependence of magnetization in nanoparticle sys-

tems, as the low-energy SW excitations are responsible for the T-dependence of the magnetization.

1.7.2 Discretized Spectra

A significant effect of the imposition of a finite length scale is the discretization of the SW spectra [10]. Again, while we examine the full SW spectra of our system, of particular interest are the low energy states. Even a system with zero magnetic anisotropy will have a non-zero energy difference between ground and first excited state:

$$\hbar\omega_0 = \frac{4\pi^2 JSa^2}{d^2}, \tag{1.10}$$

where d is the diameter of the nanoparticle and the last equality holds for a FM (Eq. (1.2) with $q = \Delta q$) [10]. This energy gap can be on the order of 10K, making the first excited state the only available state below T_B. This first excited state corresponds to nearly uniform ($q = 0$) precession of the spins around the easy-axis. As we will see, surface anisotropy significantly impacts the behaviour of these uniform excitation modes.

1.7.3 Surface Modes

Measurements of ferromagnetic resonance (FMR) in thin films have shown the appearence of surface SW modes [27]. Theory showed that the origin of these modes is due to surface magnetic anisotropy [11]. Since then, the study of these surface modes has proved a fruitful area of study [28, 29, 30]. FMR uses the coupling between an oscillatory external field and the magnetization of the sample, in concert with a perpendicularly applied DC field, to study the resonant modes of Larmor procession of the atomic spins about the direction of the DC field. Studies have shown that EP surface anisotropy leads to low-frequency "acoustic" modes, in which the amplitudes of the precession cones vary monotonically from the largest value at the surface, to the lowest value at the film centre. These acoustic modes result, in part, from the distortion of the ω_0 uniform modes by the EP anisotropy. EA anisotropy leads to high-frequency "optical" modes, where the magnitude of the precession cones varies monotonically in the same manner as the acoustic modes, but in which the precession of adjacent layers are 180° out-of-phase with one another. Optical modes require rela-

tively large EA anisotropy and result from the distortion of the high-frequency modes.

The spin dynamics of magnetic thin films subject to surface anisotropy can be described by modelling one-dimensional spin chains perpendicular to the film's plane. In that case surface anisotropy becomes edge anisotropy for the 1d chains [11]. The interaction between spin chains leads to dispersion of the surface modes.

In summary, this chapter provided context for the problem that we tackle in this thesis: The impact of edge anisotropy on the SW excitations of one-dimensional spin chains. We hope solving this problem will provide insight into the magnetic excitations of nanoparticles as well as thin films.

Chapter 2

Theory of Spin Waves in a Finite System

While we considered several approaches to examining the behaviour of magnons in nanoparticles, including an in-depth investigation of the equations of motion of semi-classical spins, we settled on the investigation of the scattering function as the best tool for tackling the problem outlined in the previous chapter. The primary benefit of this approach is its translation to experimental results. The scattering function is the physical quantity measured in inelastic neutron scattering. We hope that by outlining a method to evaluate the scattering function of a finite magnetic system with edge-anisotropy, we will provide an invaluable tool to experimental physicists and theoreticians alike.

The evaluation of the scattering function for magnetic systems is non-trivial; however, we can draw heavily upon previous work evaluating the scattering function of bulk magnetic materials [1]. Infinite (bulk) systems have translational symmetry of the atomic sites, so that the application of a spatial Fourier transform leads to a diagonal Hamiltonian. Restricting our system to finite sizes destroys the translational symmetry at the edges, so that Fourier transformation alone is not sufficient to diagonalize the Hamiltonian. The first contribution of this work is the development of a framework to evaluate the scattering function of a magnetic system that is not translation invariant.

The second contribution of this work is the inclusion of an edge-anisotropy term in the Hamiltonian of the system. As outlined in the previous chapter, recent works have led us to believe that edge-anisotropy may play a significant role in the dynamic behaviour of magnetic nanoparticles. The development of a framework for evaluating the scattering function of finite magnetic systems will allow us to understand the

impact of edge anisotropy on the spin wave excitations.

The following sections of this chapter will first detail the evaluation of the scattering function for finite systems. Following this, we will apply our framework to four case studies; a 1D FM chain with periodic boundary conditions, a 1D FM chain with edge-anisotropy, a 1D AFM chain with periodic boundary conditions, and a 1D AFM chain with edge-anisotropy. These case studies will serve a three-fold purpose; they will serve as validation of our approach as well as tutorials in the application of our framework. Thirdly, they will probe the effects of finite-size and edge-anisotropy on the dynamic behaviour of magnetic nanoparticles.

2.1 Method to Evaluate the Scattering Function for Finite Systems

The scattering function of a magnetic system is the space and time Fourier transform of the time-dependent spin-spin correlation function,

$$S_{\alpha\beta}(\boldsymbol{q},\omega) = \frac{1}{2\pi N}\sum_{i,j}\int dt e^{-i\omega t} e^{-i\boldsymbol{q}\cdot(\boldsymbol{R}_i-\boldsymbol{R}_j)} \left\langle \hat{S}_i^{\alpha}(0)\hat{S}_j^{\beta}(t)\right\rangle_T . \tag{2.1}$$

In this equation, $\boldsymbol{q}$ is proportional to the scattering momentum $\hbar\boldsymbol{\kappa}$ of the scattered neutron, and ω is proportional to the energy transfer $\hbar\omega$ of the scattered neutron. N is the number of sites, $\boldsymbol{R}_i$ and $\boldsymbol{R}_j$ are the positions of sites i and j, and $\hat{S}_i^{\alpha}$ and $\hat{S}_j^{\beta}$ are the cartesian components of the spin operators at sites i and j ($\alpha,\beta = x,y,z$). $S_{\alpha\beta}(\boldsymbol{q},\omega)$ corresponds to the creation of excitations along $\boldsymbol{\alpha}$ due to scattering in $\boldsymbol{\beta}$.

It should be possible to evaluate $S_{\alpha\beta}(\boldsymbol{q},\omega)$ based on our framework for any α and β, however, without adding simplifying assumptions to the system, we must repeat the process for each unique combination of α and β. We, therefore, limit ourselves to collinear systems such as a Heisenberg FM or AFM where the spins are aligned along $\pm\boldsymbol{z}$, and the total spin along $\boldsymbol{z}$ is a constant of motion. This restriction means $S_{\alpha\beta}(\boldsymbol{q},\omega) = 0$ for $\alpha \neq \beta$, $S_{xx}(\boldsymbol{q},\omega) = S_{yy}(\boldsymbol{q},\omega)$, and $S_{zz}(\boldsymbol{q},\omega) = 0$. We will limit ourselves to the examination of $S_{xx}(\boldsymbol{q},\omega)$, which corresponds to the creation of spin waves.

The crux of the analysis is evaluating the correlation function, which requires determining the energy eigenstates of the system, which in turn requires solving the

EOM, and then finally, transforming the spin operators to the energy eigenstate basis. Once we have achieved this, it is just a matter of evaluating,

$$\begin{aligned}\langle \hat{S}_i^x(0)\hat{S}_j^x(t)\rangle_T &= \sum_{n,n'} \frac{\mathrm{e}^{-\frac{E_n}{k_B T}}}{Z} \langle n|\hat{S}_i^x(0)|n'\rangle \langle n'|\hat{S}_j^x(t)|n\rangle \,, \\ &= \sum_{n,n'} \frac{\mathrm{e}^{-\frac{E_n}{k_B T}}}{Z} \langle n|\hat{S}_i^x(0)|n'\rangle \langle n'|e^{i\hat{\mathcal{H}}t/\hbar}\hat{S}_j^x(0)e^{-i\hat{\mathcal{H}}t/\hbar}|n\rangle \,,\end{aligned} \tag{2.2}$$

where $Z = \sum_n \mathrm{e}^{-\frac{E_n}{k_B T}}$ is the partition function, and n and n' sum over the eigenstates of the system.

The first task will be determining the EOM of our system. To study the dynamic behaviour of a magnetic system, we can describe our system via a Heisenberg Hamiltonian,

$$\hat{\mathcal{H}} = -\sum_{i,j} J_{\boldsymbol{r_{ij}}} \hat{\boldsymbol{S}}_i \cdot \hat{\boldsymbol{S}}_j. \tag{2.3}$$

Here i and j sum over all atomic sites, $\hat{\boldsymbol{S}}_i$ and $\hat{\boldsymbol{S}}_j$ are the spin operators at the i_{th} and j_{th} sites, and $J_{\boldsymbol{r_{ij}}}$ is the coupling constant between these spins. We further simplify by assuming $J_{\boldsymbol{r_{ij}}}$ is negligible beyond nearest-neighbour spins, and that it is constant, regardless of direction. These simplifications leave us with

$$\hat{\mathcal{H}} = -J \sum_{<i,j>} \hat{\boldsymbol{S}}_i \cdot \hat{\boldsymbol{S}}_j, \tag{2.4}$$

where $< i, j >$ corresponds to the summation over nearest neighbours.

We expand the spin operators as $\hat{\boldsymbol{S}}_i \cdot \hat{\boldsymbol{S}}_j = \hat{S}_i^z \cdot \hat{S}_j^z + \frac{1}{2}(\hat{S}_i^+ \hat{S}_j^- + \hat{S}_i^- \hat{S}_j^+)$, where S_i^+ and S_i^- are the spin raising and lowering operators respectively, and an operator $\hat{S}_i^\alpha$ acts on a state of the form $|j_i, m_i\rangle$. Here $j_i = S_i$ is the total spin at the site i, and m_i is the magnetic spin quantum number. We can write the possible values of m_i as $m_i = j_i - m_i'$, where $m_i' = 0, 1, ..., 2j_i$. We can simplify our system by applying the constraint $S_i = S \; \forall i$, allowing us to write $|j_i, m_i\rangle = |m_i'\rangle$, where $m_i' = 0, 1, ..., 2S$.

One method for determining the eigenstates of this system would be to diagonal-

ize the matrix representation of $\hat{\mathcal{H}}$ using the basis formed by the direct products of the states $|m_i'\rangle$ corresponding to the state of each spin. This approach results in a $(2S+1)^N$ dimensional Hilbert space, for which diagonalization of $\hat{\mathcal{H}}$, even for $S = 1/2$, becomes computationally unfeasible for $N > 15$. We use the Holstein-Primakoff (HP) representation to reduce the computational cost of eigendecomposition significantly.

2.1.1 The Holstein-Primakoff Representation

The HP representation boils down to a second quantization representation of the spin states and operators. In the second quantization, we are still trying to solve

$$\hat{\mathcal{H}} |n\rangle = E_n |n\rangle , \tag{2.5}$$

but we re-write $\hat{\mathcal{H}}$ in terms of creation and annihilation operators, for which $\{|n\rangle\}$ are the eigenstates. The classic example is expressing the Hamiltonian of the simple harmonic oscillator in terms of the creation and annihilation operators $\hat{a}^\dagger$ and $\hat{a}$. We search for a similar representation for our Heisenberg Hamiltonian.

We begin by examining the case of a single spin, and use the $\hat{S}^z$ operator as a starting point and will work outwards from there. We know

$$\begin{aligned} \hat{S}^z |j, m\rangle &= \hbar m |j, m\rangle , \\ &= \hbar m |m'\rangle \\ &= \hbar(S - m') |m'\rangle \\ &= S^z |m'\rangle \end{aligned} \tag{2.6}$$

Drawing from the SHO, we write this as

$$\hat{S}^z |m'\rangle = \hbar(S - \hat{a}^\dagger \hat{a}) |m'\rangle . \tag{2.7}$$

We deduce that the occupation number m' for the number of particles, which $\hat{a}^\dagger \hat{a}$ counts, indicates the number of excitation in the spin. It follows that

$$\begin{aligned}
\hat{a}\,|m'\rangle &= \sqrt{m'}\,|m'-1\rangle\,, \quad 1 \leq m' \leq 2S \\
\hat{a}^\dagger\,|m'\rangle &= \sqrt{m'+1}\,|m'+1\rangle \quad 0 \leq m' \leq 2S-1 \\
[\hat{a}, \hat{a}^\dagger] &= 1.
\end{aligned} \tag{2.8}$$

In order to write Eq. 2.4 in the HP representation, we must also determine the form of $\hat{S}^+$ and $\hat{S}^-$. Making use of the fact that,

$$\hat{S}^+\,|j,m\rangle = \hbar\sqrt{(j-m)(j+m+1)}\,|j,m+1\rangle\,, \tag{2.9}$$

we can show,

$$\begin{aligned}
\hat{S}^+\,|m'\rangle &= \hbar\sqrt{2S-(m'-1)}\sqrt{m'}\,|m'-1\rangle\,, \\
\hat{S}^+ &= \hbar\sqrt{2S-\hat{a}^\dagger\hat{a}}\,\hat{a}, \\
\hat{S}^- &= \hbar\hat{a}^\dagger\sqrt{2S-\hat{a}^\dagger\hat{a}},
\end{aligned} \tag{2.10}$$

where we made use of the fact that $\hat{S}^- = (\hat{S}^+)^\dagger$. So $\hat{a}^\dagger$ creates a Holstein-Primakoff boson, which is interpreted as a spin-flip excitation on top of the maximum spin state $|m = S\rangle$. $\hat{a}$ annihilates one of these excitations. We can see that $\hat{S}^+$ annihilates HP bosons, while $\hat{S}^-$ creates HP bosons. Finally, we can write

$$\begin{aligned}
\hat{S}^x &= \hbar\frac{\sqrt{2S-\hat{a}^\dagger\hat{a}}\,\hat{a} + \hat{a}^\dagger\sqrt{2S-\hat{a}^\dagger\hat{a}}}{2}, \\
\hat{S}^y &= \hbar\frac{\sqrt{2S-\hat{a}^\dagger\hat{a}}\,\hat{a} - \hat{a}^\dagger\sqrt{2S-\hat{a}^\dagger\hat{a}}}{2i},
\end{aligned} \tag{2.11}$$

from which we can show,

$$[\hat{S}^\alpha, \hat{S}^\beta] = i\hbar\epsilon^{\alpha\beta\gamma}\hat{S}^\gamma, \tag{2.12}$$

thus, the HP representation preserves the physics of the system. Eqs. 2.7 and 2.11 are the constituent elements of the HP representation. The $|m' = 0\rangle$ ground state is called vacuum and has $m = S$; in other words, all the spin aligns along $\boldsymbol{z}$. We generate a state $|m'\rangle$ from the ground state via,

$$|m'\rangle = \hat{\Lambda}\frac{(\hat{a}^\dagger)^{m'}}{\sqrt{m'!}}\,|0\rangle\,, \tag{2.13}$$

where,

$$\hat{\Lambda}\,|m'\rangle = \begin{cases} |m'\rangle & \text{if } 0 \leq m' \leq 2S \\ 0 & \text{otherwise} \end{cases} \tag{2.14}$$

We can represent a collection of spins as $|m'_1, m'_2, \ldots, m'_i, \ldots, m'_N\rangle$, where m'_i is the number of HP bosons at the ith site. Operators $\hat{a}_i^\dagger$ and $\hat{a}_i$ act on the i_{th} component of $|m'_1, m'_2, \ldots\rangle$, giving

$$\begin{aligned} \hat{a}_i^\dagger\,|m'_1, m'_2, \ldots, m'_i, \ldots, m'_N\rangle &= \sqrt{m'_i + 1}\,|m'_1, m'_2, \ldots, m'_i + 1, \ldots, m'_N\rangle\,, \\ \hat{a}_i\,|m'_1, m'_2, \ldots, m'_i, \ldots, m'_N\rangle &= \sqrt{m'_i}\,|m'_1, m'_2, \ldots, m'_i - 1, \ldots, m'_N\rangle\,. \end{aligned} \tag{2.15}$$

From here, we limit ourselves to the study of single-excitation states, i.e. if $m'_i = 1$, then, $m'_j = 0$ for $j \neq i$. This is a reasonable approximation for low T, when only the lowest lying energy states play a role [17]. Limiting ourselves to single-excitation states also allows us to write Eq. 2.10 as

$$\begin{aligned} \hat{S}^+ &\approx \hbar\sqrt{2S}\hat{a}, \\ \hat{S}^- &\approx \hbar\hat{a}^+\sqrt{2S} \end{aligned} \tag{2.16}$$

provided that $S \gg 1$. It is important at this point to note that the states $|m'_1, m'_2, \ldots, m'_i, \ldots, m'_N\rangle$ are not eigenstates of the Hamiltonian in Eq. 2.4, however, equipped with our HP representation, we are now ready to tackle the eigendecomposition of our Hamiltonian.

2.1.2 Diagonalization of the Hamiltonian

In this section, we will detail the procedure used for determining the eigenstates of our Hamiltonian. However we will leave the explicit decomposition to a later section. For reasons that will soon become clear, we will need to restructure our Hamiltonian depending on whether we are studying the FM or the AFM case, meaning the explicit decomposition of either at this point would cause a loss of generality. However,

without loss of generality, we *can* expand $\hat{\mathcal{H}}$ as

$$\hat{\mathcal{H}} = \hat{\mathcal{H}}_0(S^2) + \hat{\mathcal{H}}_1(S^1) + \hat{\mathcal{H}}_2(S^0). \tag{2.17}$$

$\hat{\mathcal{H}}_0$ is the ground state energy of the system, is proportional to S^2, and does not contain any $\hat{a}_i$ or $\hat{a}_i^\dagger$ terms. As $\hat{\mathcal{H}}_0$ is a constant, it does not lend any additional information on the spin dynamics of the system, and we will, therefore, drop it. $\hat{\mathcal{H}}_1$ is the harmonic term, is proportional to S^1, and contains terms of the form $\hat{a}_i^\dagger \hat{a}_j$. $\hat{\mathcal{H}}_1$ corresponds to the energies of single excitations and, therefore, will be the focus of our study. $\hat{\mathcal{H}}_2$ is the anharmonic term, is proportional to S^0, and contains terms of the form $\hat{a}_i^\dagger \hat{a}_j \hat{a}_k^\dagger \hat{a}_l$. $\hat{\mathcal{H}}_2$ describes the mutual interaction between excitations in the system. This term is negligible at low T when the number of thermally activated magnons is small. For this reason, we also drop $\hat{\mathcal{H}}_2$ and focus entirely on $\hat{\mathcal{H}}_1$. We note that if we divide Eq. 2.17 by S^2, it becomes an expansion in powers of $1/S$. Therefore, neglecting $\mathcal{H}_2$ is equivalent to dropping the $1/S^2$ contribution. Evidently this becomes a good approximation in the limit $S \gg 1$.

It is convenient to write $\hat{\mathcal{H}}_1$ in matrix form,

$$\hat{\mathcal{H}}_1 = \hat{\boldsymbol{V}}^\dagger \underline{L} \hat{\boldsymbol{V}}, \tag{2.18}$$

where $\hat{\boldsymbol{V}}^\dagger = \left(\hat{a}_1^\dagger, \hat{a}_2^\dagger, \ldots, \hat{a}_N^\dagger | \hat{a}_1, \hat{a}_2, \ldots, \hat{a}_N\right)$, and $\hat{\boldsymbol{V}} = \left(\hat{\boldsymbol{V}}^\dagger\right)^{*^T}$. $\underline{L}$ is a Hermitian $2N \times 2N$ matrix with the property,

$$\underline{L} = \begin{bmatrix} \underline{P} & \underline{Q} \\ \underline{Q} & \underline{P} \end{bmatrix}, \tag{2.19}$$

where $\underline{P}$ and $\underline{Q}$ are $N \times N$ matrices. The form of $\hat{\boldsymbol{V}}^\dagger$ is chosen to allow the symmetry arguments of 2.19 to be satisfied.

Here we have made our first departure from the conventional bulk approach to evaluating the scattering function. In the bulk approach, at this point, we would apply a Fourier transform to $\underline{L}$, reducing it to a $2u \times 2u$ matrix that depends on $\boldsymbol{q}$, where u is the number of sites in the magnetic unit cell along $\boldsymbol{x}$. In the bulk case, one ensures the symmetry requirements of Eq. 2.19 are satisfied by including both $\boldsymbol{q}$ and $-\boldsymbol{q}$ terms in the Hamiltonian. Due to the lack of translational symmetry in our

finite system, we must use the real space representation of $\underline{L}$. We, therefore, we will be required to determine an equivalent form of $-\boldsymbol{q}$ in the real space representation. We go over how we achieve this when we deal with the FM and AFM cases explicitly, for now we assume $\underline{L}$ has the necessary form.

The next step is to assume the behaviour of $\hat{a}_i^\dagger$ and $\hat{a}_i$ will be oscillatory, which allows us to write,

$$\hat{a}_i(t) = \hat{a}_i(0)e^{-i\omega t} \quad \text{and} \quad \hat{a}_i^\dagger(t) = \hat{a}_i^\dagger(0)e^{i\omega t}. \tag{2.20}$$

Our next step is to diagonalize the equations of motion (EOM) of $\hat{\boldsymbol{V}}$ given by

$$i\hbar\frac{d\hat{\boldsymbol{V}}}{dt} = -[\hat{\mathcal{H}}_1, \hat{\boldsymbol{V}}] = \underline{\mathcal{L}}\hat{\boldsymbol{V}}, \tag{2.21}$$

where $\underline{\mathcal{L}} = \underline{NL}$ and $\underline{N} = \begin{bmatrix} \underline{I} & \underline{0} \\ \underline{0} & -\underline{I} \end{bmatrix}$. The eigenvalues of $\underline{\mathcal{L}}$ are

$$\epsilon_n = \begin{cases} \hbar\omega_n/2 & \text{if } n \in (1, N) \\ -\hbar\omega_{n-N}/2 & \text{if } n \in (N+1, 2N), \end{cases} \tag{2.22}$$

where N is the number of spins in the system. It is important to note here that ϵ_n are not the energy eigenvalues of the Hamiltonian, but of the EOM.

We diagonalize $\underline{\mathcal{L}}$ using unitary transformation $\underline{\mathcal{L}}' = \underline{U\mathcal{L}U}^\dagger$, with the columns of $\underline{U}^\dagger$ being the eigenvectors of $\underline{\mathcal{L}}$, which we will denote by $\boldsymbol{u}_n$. We diagonalize $\hat{\mathcal{H}}_1$ by transforming it via,

$$\hat{\mathcal{H}}_1 = \hat{\boldsymbol{V}}^\dagger\underline{U}^\dagger\underline{ULU}^\dagger\underline{U}\hat{\boldsymbol{V}} = \hat{\boldsymbol{W}}^\dagger\underline{L}'\hat{\boldsymbol{W}}, \tag{2.23}$$

where $\hat{\boldsymbol{W}}^\dagger = \hat{\boldsymbol{V}}^\dagger\underline{U}^\dagger = \left(\hat{\alpha}_1^\dagger, \hat{\alpha}_2^\dagger, \ldots, \hat{\alpha}_N^\dagger | \hat{\alpha}_1, \hat{\alpha}_2, \ldots, \hat{\alpha}_N\right)$. Here $\hat{\alpha}_n^\dagger$ and $\hat{\alpha}_n$ are boson creation and annihilation operators respectively, satisfying $[\hat{\alpha}_n, \hat{\alpha}_{n'}^\dagger] = \delta_{n,n'}$. Expanding $\hat{\mathcal{H}}_1$ on this new basis, we have,

$$\hat{\mathcal{H}}_1 = \sum_{n=1}^{N} \frac{\hbar\omega_n}{2}\left(\hat{\alpha}_n^\dagger\hat{\alpha}_n + \hat{\alpha}_n\hat{\alpha}_n^\dagger\right) = \hbar\sum_{n=1}^{N}\omega_n(\hat{\alpha}_n^\dagger\hat{\alpha}_n + \frac{1}{2}). \tag{2.24}$$

Noting that we can express $\hat{\alpha}_n^\dagger$ and $\hat{\alpha}_n$ as

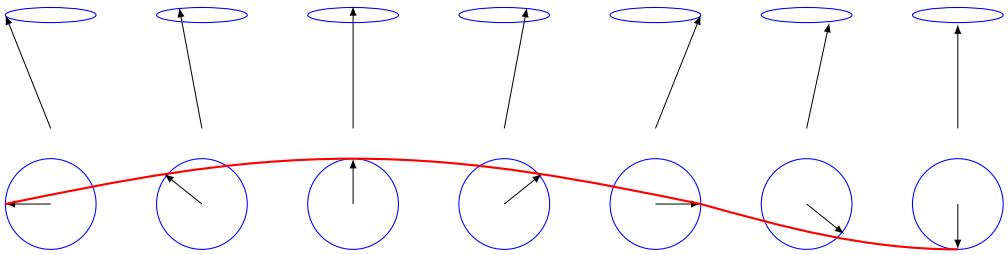

Figure 2.1: Side and top view of spins in a SW

$$\begin{aligned}\hat{\alpha}_n^\dagger &= \sum_{i=1}^{N} \left(u_{i,n}^\dagger \hat{a}_i^\dagger + u_{i+N,n}^\dagger \hat{a}_i \right), \\ \hat{\alpha}_n &= \sum_{i=1}^{N} \left(u_{i,n+N}^\dagger \hat{a}_i^\dagger + u_{i+N,n+N}^\dagger \hat{a}_i \right),\end{aligned} \tag{2.25}$$

where $u_{ij}^\dagger = \left[U^\dagger\right]_{ij}$, it becomes clear that $\hat{\alpha}_n^\dagger$ and $\hat{\alpha}_n$ create and annihilate oscillating collective excitations with energy $\hbar\omega_n$, i.e.,

$$\begin{aligned}\hat{\alpha}_n^\dagger \left|0\right\rangle &= \left|n\right\rangle, \\ \hat{\alpha}_n \left|n\right\rangle &= \left|0\right\rangle.\end{aligned} \tag{2.26}$$

In the FM with periodic b.c., these SWs are superpositions of forward and backward propagating waves, leading to the sinusoidal form shown in Fig. 2.1.

As we shall see in the solution for the FM and AFM chains, a finite system has similar SW solutions but with some distortion to the sinusoids.

2.1.3 Calculation of the Scattering Function

Now that we have determined how to evaluate the energy eigenstates of the system, we recall,

$$\hat{S}_i^x = \hbar \frac{\sqrt{2S}(\hat{a}_i + \hat{a}_i^\dagger)}{2}, \tag{2.27}$$

and that the goal of this whole procedure was to evaluate,

$$\langle \hat{S}_i^x(0)\hat{S}_j^x(t)\rangle_T = \sum_{n,n'} \frac{\mathrm{e}^{-\frac{E_n}{k_B T}}}{Z} \langle n|\hat{S}_i^x(0)|n'\rangle \langle n'|\hat{S}_j^x(0)|n\rangle \, e^{i(E_n - E'_n)t/\hbar}, \tag{2.28}$$

we transform $\hat{a}_i$ and $\hat{a}_i^\dagger$ to the eigenstate bases ($\hat{\alpha}_n$ and $\hat{\alpha}_n^\dagger$ operators) via,

$$\vec{\hat{V}} = \underline{U}^\dagger \vec{\hat{W}} \implies \hat{V}_i = \begin{cases} \hat{a}_i = \sum_{n=1}^{N} \left(u_{i,n}^\dagger \hat{\alpha_n} + u_{i,n+N}^\dagger \hat{\alpha_n}^\dagger \right) & \text{if } i \in (1, N) \\ \hat{a}_{i-N}^\dagger = \sum_{n=1}^{N} \left(u_{i,n}^\dagger \hat{\alpha_n} + u_{i,n+N}^\dagger \hat{\alpha_n}^\dagger \right) & \text{if } i \in (N+1, 2N) \end{cases}. \tag{2.29}$$

These transformations allow us to write

$$\hat{S}_i^x(0) = \hbar \frac{\sqrt{2S}}{2} (\hat{a}_i + \hat{a}_i^\dagger) = \hbar \frac{\sqrt{2S}}{2} \sum_{n=1}^{N} \left[\hat{\alpha}_n \underbrace{(u_{i,n}^\dagger + u_{i+N,n}^\dagger)}_{X_1(i,n)} + \hat{\alpha}_n^\dagger \underbrace{(u_{i,n+N}^\dagger + u_{i+N,n+N}^\dagger)}_{X_2(i,n)} \right] \tag{2.30}$$

and

$$\hat{S}_j{}^x(t) = \hbar \frac{\sqrt{2S}}{2} \sum_{n=1}^{N} \left[\mathrm{e}^{-i\omega_n t} \hat{\alpha}_n X_1(j,n) + \mathrm{e}^{i\omega_n t} \hat{\alpha}_n^\dagger X_2(j,n) \right]. \tag{2.31}$$

Inserting these into Eq. 2.28 for the spin-spin correlation function we get,

$$\begin{aligned} \langle \hat{S}_i^x(0)\hat{S}_j^x(t)\rangle_T = \hbar^2 \frac{S}{2} \sum_{n,n'} \frac{\mathrm{e}^{-\frac{E_n}{k_B T}}}{Z} & \langle n|\hat{\alpha}_n X_1(i,n) + \hat{\alpha}_n^\dagger X_2(i,n)|n'\rangle \\ & \langle n'|\mathrm{e}^{-i\omega_n t}\hat{\alpha}_n X_1(j,n) + \mathrm{e}^{i\omega_n t}\hat{\alpha}_n^\dagger X_2(j,n)|n\rangle . \end{aligned} \tag{2.32}$$

As we are restricting ourselves to single-excitation states, if $n \neq 0$ then $n' = 0$ and vice versa. Therefore,

$$\langle n'|\hat{\alpha}_n|n\rangle \begin{cases} \neq 0 & \text{if } n'=0 \\ =0 & \text{otherwise} \end{cases}$$
$$\langle n|\hat{\alpha}_n^\dagger|n'\rangle \begin{cases} \neq 0 & \text{if } n'=0 \\ =0 & \text{otherwise} \end{cases} . \tag{2.33}$$

Using these conditions along with the commutation relation $[\hat{\alpha}_n, \hat{\alpha}_n^\dagger] = 1$, and

$$\frac{\mathrm{e}^{-\frac{E_n}{k_B T}}}{Z} \langle \hat{\alpha_n}^\dagger \hat{\alpha}_n \rangle = n_B(\omega_n), \tag{2.34}$$

where $n_B(\omega_n)$ is the boson occupation function given by,

$$n_B(\omega_n) = \frac{1}{e^{\hbar\omega_n/k_B T} - 1}, \tag{2.35}$$

we can finally write the scattering function as,

$$\langle \hat{S}_i^x(0)\hat{S}_j^x(t)\rangle_T = \hbar^2 \frac{S}{2} \sum_n \left[X_1(i,n)X_2(j,n)(n_B(\omega_n)+1)e^{i\omega_n t} + X_2(i,n)X_1(j,n)n_B(\omega_n)e^{-i\omega_n t} \right]. \tag{2.36}$$

Inserting this into Eq. 2.1 for the scattering function we have,

$$\begin{aligned} S_{\alpha,\beta}(\vec{q},\omega) =& \hbar^2 \frac{S}{4\pi N} \sum_{i,j} \sum_n \int dt e^{-i\vec{q}\cdot(\vec{R}_i - \vec{R}_j)} \big[X_1(i,n)X_2(j,n)(n_B(\omega_n)+1)e^{-i(\omega-\omega_n)t} \\ &+ X_2(i,n)X_1(j,n)n_B(\omega_n)e^{-i(\omega+\omega_n)t} \big]. \end{aligned} \tag{2.37}$$

When we integrate over t, $e^{-i(\omega\pm\omega_n)t} \to \delta(\omega \pm \omega_n)$, and assuming $\omega > 0$, $\delta(\omega + \omega_n) = 0 \; \forall \; \omega$. $S_{xx}(\vec{q},\omega)$ can then be expressed as,

$$\boxed{S_{\alpha,\beta}(\vec{q},\omega) = \hbar^2 \frac{S}{2N} \sum_{i,j} \sum_n e^{-i\vec{q}\cdot(\vec{R}_i - \vec{R}_j)} X_1(i,n)X_2(j,n)(n_B(\omega_n)+1)\delta(\omega-\omega_n).} \tag{2.38}$$

The next step is to look at specific spin configurations and Hamiltonians to de-

termine the values of ω_n, $X_1(i,n)$, and $X_2(i,n)$ through the process of eigendecomposition outlined above.

2.2 Applications: FM and AFM Chains with and without Boundary Conditions

We will now go over the case studies of a 1D FM spin chain and a 1D AFM spin chain. For each case, we will analyze the system with both periodic and open boundary conditions, and with both bulk and edge anisotropy in the latter case. Using periodic boundary conditions will allow us to quantify the effects of finite-size better. These are toy models that serve two purposes. First, they provide examples of how to apply the procedure outlined in the previous section. Second, they serve as an initial glimpse into the types of behaviours we may expect the finite size and edge anisotropy to have in higher dimensional analysis. In this section, we will determine the form of the $\underline{L}$ matrix for each case. Determining the form of L is by far the most challenging step in the analysis. Once we have the form of L, the final steps are to perform the eigendecomposition and insert the results into Eq. 2.38. The results of which are presented and analyzed in the next two chapters.

2.2.1 FM with Periodic Boundary Conditions

We begin our investigation of the behaviour of SW excitations in finite systems with the most straightforward conceivable system, the 1D ferromagnetic chain with periodic boundary conditions where we consider only nearest-neighbour interactions.

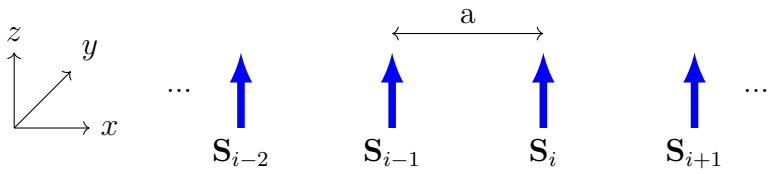

The Hamiltonian for a 1D ferromagnetic chain with periodic boundary conditions is given by

$$\hat{\mathcal{H}} = -J \sum_{i=1}^{N} \hat{\mathbf{S}}_i \cdot \hat{\mathbf{S}}_{i+1}. \tag{2.39}$$

If we were to expand Eq. 2.39 and apply the HP transformation, it would not satisfy the symmetry requirements of Eq. 2.19. We, therefore, split the Hamiltonian into two parts,

$$\hat{\mathcal{H}} = -\frac{1}{2}J\sum_{i=1}^{N}\hat{\mathbf{S}}_i\cdot\hat{\mathbf{S}}_{i+1} - \frac{1}{2}J\sum_{i=1}^{N}\hat{\mathbf{S}}_i\cdot\hat{\mathbf{S}}_{i-1}. \tag{2.40}$$

Including the $\hat{\mathbf{S}}_i\cdot\hat{\mathbf{S}}_{i-1}$ terms is the real space equivalent of including $-\boldsymbol{q}$ terms in the momentum space Hamiltonian. Expanding $\hat{\mathcal{H}}$ we get

$$\begin{aligned}\hat{\mathcal{H}} = &-\frac{1}{2}J\sum_{i=1}^{N}\left(\hat{S}_i^z\cdot\hat{S}_{i+1}^z + \frac{1}{2}(\hat{S}_i^+\hat{S}_{i+1}^- + \hat{S}_i^-\hat{S}_{i+1}^+)\right)\\ &-\frac{1}{2}J\sum_{i=1}^{N}\left(\hat{S}_i^z\cdot\hat{S}_{i-1}^z + \frac{1}{2}(\hat{S}_i^+\hat{S}_{i-1}^- + \hat{S}_i^-\hat{S}_{i-1}^+)\right)\end{aligned} \tag{2.41}$$

Employing the HP transformation, we then write the Hamiltonian as

$$\begin{aligned}\hat{\mathcal{H}} =& -\hbar^2\frac{J}{2}\sum_{i=1}^{N}\left((S-\hat{a}_i^\dagger\hat{a}_i)(S-\hat{a}_{i+1}^\dagger\hat{a}_{i+1}) + \frac{1}{2}2S(\hat{a}_i\hat{a}_{i+1}^\dagger + \hat{a}_i^\dagger\hat{a}_{i+1})\right)\\ &-\hbar^2\frac{J}{2}\sum_{i=1}^{N}\left((S-\hat{a}_i^\dagger\hat{a}_i)(S-\hat{a}_{i-1}^\dagger\hat{a}_{i-1}) + \frac{1}{2}2S(\hat{a}_i\hat{a}_{i-1}^\dagger + \hat{a}_i^\dagger\hat{a}_{i-1})\right)\\ \hat{\mathcal{H}} =& -\hbar^2\frac{J}{2}\sum_{i}^{N}\left\{S^2 - S\hat{a}_i^\dagger\hat{a}_i - S\hat{a}_{i+1}^\dagger\hat{a}_{i+1} + S\hat{a}_i\hat{a}_{i+1}^\dagger + S\hat{a}_i^\dagger\hat{a}_{i+1} + \hat{a}_i^\dagger\hat{a}_i\hat{a}_{i+1}^\dagger\hat{a}_{i+1}\right\}\\ &-\hbar^2\frac{J}{2}\sum_{i}^{N}\left\{S^2 - S\hat{a}_i^\dagger\hat{a}_i - S\hat{a}_{i-1}^\dagger\hat{a}_{i-1} + S\hat{a}_i\hat{a}_{i-1}^\dagger + S\hat{a}_i^\dagger\hat{a}_{i-1} + \hat{a}_i^\dagger\hat{a}_i\hat{a}_{i-1}^\dagger\hat{a}_{i-1}\right\}\\ =&\underbrace{-\hbar^2JNS^2}_{\hat{\mathcal{H}}_0} + \underbrace{\hbar^2\frac{JS}{2}\sum_{i=1}^{N}\left(2\hat{a}_i^\dagger\hat{a}_i + \hat{a}_{i+1}^\dagger\hat{a}_{i+1} + \hat{a}_{i-1}^\dagger\hat{a}_{i-1} - \hat{a}_i\hat{a}_{i+1}^\dagger - \hat{a}_i^\dagger\hat{a}_{i+1} - \hat{a}_i\hat{a}_{i-1}^\dagger - \hat{a}_i^\dagger\hat{a}_{i-1}\right)}_{\hat{\mathcal{H}}_1}\\ &+\underbrace{\mathcal{O}(S^0)}_{\hat{\mathcal{H}}_2}.\end{aligned} \tag{2.42}$$

As outlined in the previous section, $\hat{\mathcal{H}}$ is expanded into terms proportional to S^2, S^1, and S^0. As expected, $\hat{\mathcal{H}}_0 = -\hbar^2JNS^2$, the classical ground state energy of a 1D ferromagnetic chain.

We can then write $\hat{\mathcal{H}}_1$ in matrix form $\hat{\mathcal{H}}_1 = \vec{\hat{V}}^\dagger \underline{L} \vec{\hat{V}}$ with

$$\underline{L} = \hbar^2 \frac{JS}{2} \begin{bmatrix} \underline{P} & \underline{0} \\ \underline{0} & \underline{P} \end{bmatrix} \quad \text{and} \quad \underline{P} = \begin{bmatrix} 2 & -1 & 0 & 0 & \dots & -1 \\ -1 & 2 & -1 & 0 & \dots & 0 \\ 0 & -1 & 2 & -1 & \dots & 0 \\ \vdots & \vdots & \ddots & & \ddots & \\ 0 & 0 & 0 & -1 & 2 & -1 \\ -1 & 0 & 0 & 0 & -1 & 2 \end{bmatrix}. \tag{2.43}$$

2.2.2 FM with Open Boundary Conditions, Bulk, and Edge Anisotropy

The first complication we introduce to the system is open boundary conditions with bulk EA anisotropy, along with an edge anisotropy term. We arbitrarily choose the axis of alignment to be the z axis. However, this does not cause a loss of generality. The Hamiltonian then reads,

$$\hat{\mathcal{H}} = -\frac{1}{2} J \sum_{i=1}^{N-1} \hat{\mathbf{S}}_i \cdot \hat{\mathbf{S}}_{i+1} - \frac{1}{2} J \sum_{i=2}^{N} \hat{\mathbf{S}}_i \cdot \hat{\mathbf{S}}_{i-1} - K \sum_{i=1}^{N} (\hat{S}_i^z)^2 - K_s \left[(\hat{S}_1^z)^2 + (\hat{S}_N^z)^2 \right], \tag{2.44}$$

where we have already split the exchange interaction terms to ensure symmetry in $\underline{L}$. The magnitudes of K and K_s describe the strength of the anisotropies, while their signs determines whether the interaction will be EA or EP. A positive $K_{(s)}$ forces the spins to align along $\boldsymbol{z}$ (EA), while a negative $K_{(s)}$ forces the spins to align in the xy-plane (EP). The first two terms of $\hat{\mathcal{H}}$ are identical to the periodic case except we do not include the $\hat{\mathbf{S}}_N \cdot \hat{\mathbf{S}}_1$ and $\hat{\mathbf{S}}_1 \cdot \hat{\mathbf{S}}_N$ terms. Applying the HP transformation to these two terms, we see we must subtract

$$-J(\hbar^2 S^2 - \hbar^2 S) + \frac{\hbar^2 JS}{2} \left(\hat{a}_N^\dagger \hat{a}_N + \hat{a}_N \hat{a}_N^\dagger + \hat{a}_1^\dagger \hat{a}_1 + \hat{a}_1 \hat{a}_1^\dagger - \hat{a}_N^\dagger \hat{a}_1 - \hat{a}_N \hat{a}_1^\dagger - \hat{a}_1^\dagger \hat{a}_N - \hat{a}_1 \hat{a}_N^\dagger \right) \tag{2.45}$$

from the periodic Hamiltonian. The anisotropy terms add

$$-K_s \left[(\hat{S}_1^z)^2 + (\hat{S}_N^z)^2 \right] = -2K_s(\hbar^2 S^2 - \hbar^2 S) + \hbar^2 K_s S \left(\hat{a}_N^\dagger \hat{a}_N + \hat{a}_N \hat{a}_N^\dagger + \hat{a}_1^\dagger \hat{a}_1 + \hat{a}_1 \hat{a}_1^\dagger \right), \tag{2.46}$$

and,

$$-K\sum_{i=1}^{N}(\hat{S}_i^z)^2 = -NK(\hbar^2S^2-\hbar^2S)+\hbar^2KS\sum_{i=1}^{N}\left(\hat{a}_i^\dagger\hat{a}_i+\hat{a}_i\hat{a}_i^\dagger\right)-\mathcal{O}(S^0) \tag{2.47}$$

to the periodic Hamiltonian. The resulting matrix $\underline{L}$ is

$$\underline{L}=\hbar^2\frac{JS}{2}\begin{bmatrix}\underline{P} & \underline{0}\\ \underline{0} & \underline{P}\end{bmatrix} \quad \text{where,} \quad \underline{P}=\begin{bmatrix} 1+\frac{K_s}{|J|}+\frac{K}{|J|} & -1 & 0 & 0 & \dots & 0\\ -1 & 2+\frac{K}{|J|} & -1 & 0 & \dots & 0\\ 0 & -1 & 2+\frac{K}{|J|} & -1 & \dots & 0\\ \vdots & \vdots & \ddots & & \ddots & \\ 0 & 0 & 0 & -1 & 2+\frac{K}{|J|} & -1\\ 0 & 0 & 0 & 0 & -1 & 1+\frac{K_s}{|J|}+\frac{K}{|J|}\end{bmatrix}. \tag{2.48}$$

Note that while we use $|J|$ here for consistency of notation, $J>0$ for the FM case and $J<0$ would require a different treatment.

2.2.3 AFM with Periodic Boundary Conditions

Now that we have explored a baseline system with our approach, we will now move to a more complicated system, a 1D AFM chain. The approach we use will be similar to the ferromagnetic case, but with a few alterations. We may think of the AFM as two interlaced FM sublattices, which we will call lattice A and lattice B. In the ground state of the system, these lattices have opposing magnetic ordering. We will again arbitrarily choose the z-axis as the axis of alignment. Therefore in the ground state of the system, we will have $\hat{\mathbf{S}}_m^{A(g)}=S\hat{\mathbf{z}}$ and $\hat{\mathbf{S}}_m^{B(g)}=-S\hat{\mathbf{z}}$. Here, spins in lattice A are denoted by $\hat{\mathbf{S}}_m^A$, and spins in lattice B are denoted by $\hat{\mathbf{S}}_m^B$.

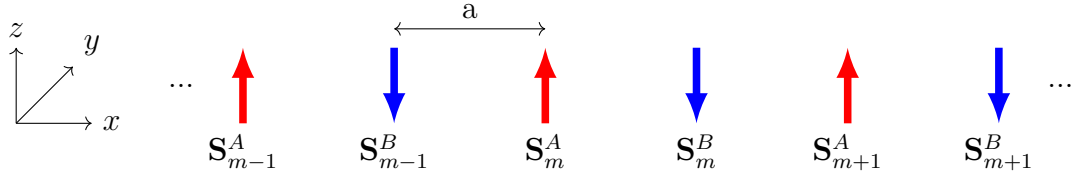

The symmetrized Hamiltonian, in this case, is given by

$$\hat{\mathcal{H}} = -\frac{J}{2}\sum_{m}^{N/2}\left(\hat{\mathbf{S}}_m^A\cdot\hat{\mathbf{S}}_m^B+\hat{\mathbf{S}}_m^A\cdot\hat{\mathbf{S}}_{m-1}^B\right)-\frac{J}{2}\sum_{m}^{N/2}\left(\hat{\mathbf{S}}_m^B\cdot\hat{\mathbf{S}}_{m+1}^A+\hat{\mathbf{S}}_m^B\cdot\hat{\mathbf{S}}_m^A\right) \tag{2.49}$$

Here the exchange interaction J must be negative for AFM order. Following a similar expansion as for the ferromagnetic case we get,

$$\begin{aligned}\hat{\mathcal{H}} =& -\frac{J}{2}\sum_{m}^{N/2}\left(\hat{S}_m^{AZ}\cdot\hat{S}_m^{BZ}+\frac{1}{2}\left[\hat{S}_m^{A+}\hat{S}_m^{B-}+\hat{S}_m^{A-}\hat{S}_m^{B+}\right]+\hat{S}_m^{AZ}\cdot\hat{S}_{m-1}^{BZ}+\frac{1}{2}\left[\hat{S}_m^{A+}\hat{S}_{m-1}^{B-}+\hat{S}_m^{A-}\hat{S}_{m-1}^{B+}\right]\right)\\ &-\frac{J}{2}\sum_{m}^{N/2}\left(\hat{S}_l^{BZ}\cdot\hat{S}_{m+1}^{AZ}+\frac{1}{2}\left[\hat{S}_m^{B+}\hat{S}_{m+1}^{A-}+\hat{S}_m^{B-}\hat{S}_{m+1}^{A+}\right]+\hat{S}_m^{BZ}\cdot\hat{S}_m^{AZ}+\frac{1}{2}\left[\hat{S}_m^{B+}\hat{S}_m^{A-}+\hat{S}_m^{B-}\hat{S}_m^{A+}\right]\right).\end{aligned} \tag{2.50}$$

At this point, we must be careful; if we wish to apply an HP transformation, we must define $\hat{S}_m^{AZ}$and $\hat{S}_m^{BZ}$ separately,

$$\begin{aligned}\hat{S}_m^{AZ} &= \hbar(S-\hat{a}_m^\dagger\hat{a}_m) \quad \hat{S}_m^{A+}\approx\hbar\sqrt{2S}\hat{a}_m \quad \hat{S}_m^{A-}\approx\hbar\sqrt{2S}\hat{a}_m^\dagger\\ \hat{S}_m^{BZ} &= \hbar(-S+\hat{b}_m^\dagger\hat{b}_m) \quad \hat{S}_m^{B+}\approx\hbar\sqrt{2S}\hat{b}_m^\dagger \quad \hat{S}_m^{B-}\approx\hbar\sqrt{2S}\hat{b}_m.\end{aligned} \tag{2.51}$$

This modification to the HP transformation is equivalent to applying a rotation, aligning the spins on lattice B along the positive $\boldsymbol{z}$ direction in their local frame. Applying the HP transformation to Eq. 2.50 for the single excitation periodic case, we get

$$\begin{aligned}\hat{\mathcal{H}} =&\hbar^2 JN(S^2-S)\\ &+\hbar^2\frac{JS}{2}\sum_{m=1}^{N/2}\left(\hat{a}_m^\dagger\hat{a}_m+\hat{a}_m\hat{a}_m^\dagger+\hat{b}_m^\dagger\hat{b}_m^\dagger+\hat{b}_m\hat{b}_m^\dagger+\hat{a}_m\hat{b}_m+\hat{a}_m^\dagger\hat{b}_m^\dagger+\hat{a}_m\hat{b}_{m-1}+\hat{a}_m^\dagger\hat{b}_{m-1}^\dagger\right)\\ &+\hbar^2\frac{JS}{2}\sum_{m=1}^{N/2}\left(\hat{b}_m^\dagger\hat{b}_m+\hat{b}_m\hat{b}_m^\dagger+\hat{a}_m^\dagger\hat{a}_m^\dagger+\hat{a}_m\hat{a}_m^\dagger+\hat{b}_m\hat{a}_m+\hat{b}_m^\dagger\hat{a}_m^\dagger+\hat{b}_m\hat{a}_{m+1}+\hat{b}_m^\dagger\hat{a}_{m+1}^\dagger\right)+\mathcal{O}\left(S^0\right),\end{aligned} \tag{2.52}$$

and $\hat{\mathcal{H}}_1 = \vec{\hat{V}}^\dagger\underline{L}\vec{\hat{V}}$ where,

$$\vec{V}^\dagger = \left(\hat{a}_1^\dagger \;\; \hat{b}_1^\dagger \;\; \hat{a}_2^\dagger \;\; \hat{b}_2^\dagger \;\; \dots \;\; \hat{a}_{N/2}^\dagger \;\; \hat{b}_{N/2}^\dagger \;\mid\; \hat{a}_1 \;\; \hat{b}_1 \;\; \hat{a}_2 \;\; \hat{b}_2 \;\; \dots \;\; \hat{a}_{N/2} \;\; \hat{b}_{N/2}\right), \tag{2.53}$$

and $\underline{L} = -\hbar^2 \frac{JS}{2} \begin{bmatrix} \underline{P} & \underline{Q} \\ \underline{Q} & \underline{P} \end{bmatrix}$, where

$$\underline{P} = \begin{bmatrix} 2 & 0 & 0 & 0 & \dots & 0 \\ 0 & 2 & 0 & 0 & \dots & 0 \\ 0 & 0 & 2 & 0 & \dots & 0 \\ \vdots & \vdots & & \ddots & & \\ 0 & 0 & 0 & 0 & 2 & 0 \\ 0 & 0 & 0 & 0 & 0 & 2 \end{bmatrix} \text{ and } \underline{Q} = \begin{bmatrix} 0 & 1 & 0 & 0 & \dots & 1 \\ 1 & 0 & 1 & 0 & \dots & 0 \\ 0 & 1 & 0 & 1 & \dots & 0 \\ \vdots & \vdots & \ddots & & \ddots & \\ 0 & 0 & 0 & 1 & 0 & 1 \\ 1 & 0 & 0 & 0 & 1 & 0 \end{bmatrix}. \tag{2.54}$$

2.2.4 AFM with Open Boundary Conditions, Bulk, and Edge Anisotropy

The Hamiltonian for the 1D antiferromagnet with bulk and edge anisotropy is given by

$$\begin{aligned} \mathcal{H} = &- \frac{J}{2} \sum_m^{N/2} \left(\hat{\mathbf{S}}_m^A \cdot \hat{\mathbf{S}}_m^B + \hat{\mathbf{S}}_m^A \cdot \hat{\mathbf{S}}_{m-1}^B\right) - \frac{J}{2} \sum_m^{N/2} \left(\hat{\mathbf{S}}_m^B \cdot \hat{\mathbf{S}}_{m+1}^A + \hat{\mathbf{S}}_m^B \cdot \hat{\mathbf{S}}_m^A\right) \\ &- K_s \left[\left(\hat{S}_1^{Az}\right)^2 + \left(\hat{S}_{N/2}^{Bz}\right)^2\right] - K \left[\sum_m^{N/2} (\hat{S}_m^{Az})^2 + (\hat{S}_m^{Bz})^2\right] \end{aligned} \tag{2.55}$$

Here, compared to the periodic case, we must subtract the terms $-\frac{J}{2}\left(\hat{\mathbf{S}}_1^A \cdot \hat{\mathbf{S}}_N^B + \hat{\mathbf{S}}_N^B \cdot \hat{\mathbf{S}}_1^A\right)$. Expanding these terms and applying the HP transformation, we see that we must subtract

$$\hbar^2 JS^2 - \frac{\hbar^2 SJ}{2}\left(2\hat{a}_1^\dagger \hat{a}_1 + 2\hat{b}_N^\dagger \hat{b}_N + \hat{a}_1 \hat{b}_N + \hat{a}_1^\dagger \hat{b}_N^\dagger + \hat{b}_N \hat{a}_1 + \hat{b}_N^\dagger \hat{a}_1^\dagger\right) \tag{2.56}$$

from the Hamiltonian for the periodic case. Expanding and applying the HP transformation to the anisotropy terms we see we must add

$$-\hbar^2 S^2 K_s + 2\hbar^2 K_s S\left(\hat{a}_1^\dagger \hat{a}_1 + \hat{b}_N^\dagger \hat{b}_N\right) \tag{2.57}$$

and,

$$-\hbar^2 NS^2K + 2\hbar^2 KS\sum_m^{N/2}\hat{a}_m^\dagger\hat{a}_m + 2\hbar^2 KS\sum_m^{N/2}\hat{b}_m^\dagger\hat{b}_m, \tag{2.58}$$

to the periodic Hamiltonian. After symmetrizing the terms, the L matrix for the open boundary conditions is $\underline{L} = -\hbar^2\frac{JS}{2}\begin{bmatrix}\underline{P} & \underline{Q}\\ \underline{Q} & \underline{P}\end{bmatrix}$, where,

$$\underline{P} = \begin{bmatrix} 1+\frac{K}{|J|}+\frac{K_s}{J} & 0 & 0 & 0 & \dots & 0\\ 0 & 2+\frac{K}{|J|} & 0 & 0 & \dots & 0\\ 0 & 0 & 2+\frac{K}{|J|} & 0 & \dots & 0\\ \vdots & \vdots & & \ddots & & \\ 0 & 0 & 0 & 0 & 2+\frac{K}{|J|} & 0\\ 0 & 0 & 0 & 0 & 0 & 1+\frac{K}{|J|}+\frac{K_s}{J}\end{bmatrix} \text{ and } \underline{Q} = \begin{bmatrix} 0 & 1 & 0 & 0 & \dots & 0\\ 1 & 0 & 1 & 0 & \dots & 0\\ 0 & 1 & 0 & 1 & \dots & 0\\ \vdots & \vdots & \ddots & & \ddots & \\ 0 & 0 & 0 & 1 & 0 & 1\\ 0 & 0 & 0 & 0 & 1 & 0\end{bmatrix}. \tag{2.59}$$

Here we use $|J|$, however, it is important to note the $J < 0$, and that the $J > 0$ case requires a different treatment.

In this chapter we first developed a method for evaluating the scattering function of 1D finite systems. We then applied this method to our four case studies; periodic FM and AFM systems as well as finite FM and AFM systems with bulk and edge anisotropy. We are left with the matrix representation of the Hamiltonians of the case studies. In the following two chapters we diagonalize these Hamiltonians, and use the results to evaluate the scattering function of each case study.

Chapter 3

Numerical Results for the Ferromagnetic Chain

This chapter first outlines the technical steps taken between determining the form of the $\underline{L}$ matrices, and the plotting of the scattering function. We then present and analyze the results for the FM cases.

We implement our analysis in Matlab due to its strong performance in matrix diagonalization; however, any software/language capable of diagonalization of large matrices should suffice. Our end step is plotting

$$\boxed{S_{x,x}(\boldsymbol{q},\omega) = \hbar^2 \frac{S}{2N} \sum_{i,j} \sum_{n} e^{-i\boldsymbol{q}\cdot(\boldsymbol{R}_i - \boldsymbol{R}_j)} X_1(i,n) X_2(j,n) (n_B(\omega_n)+1) \delta(\omega - \omega_n).} \tag{3.1}$$

The steps once we have determined the form of $\underline{L}$, are as follows,

1. First, we are working with toy models in our 1D chains and not modelling real physical systems. Therefore, we are more interested in overall behaviour than exact physical quantities. To this end, we will work in reduced units, setting $S = J = \hbar = 1$. We also set the atomic spacing a to $a = 1$, allowing us to write $\boldsymbol{R}_i - \boldsymbol{R}_j = a(i-j) = (i-j)$.

2. Second, we diagonalize $\underline{\mathcal{L}} = \underline{L} \cdot \underline{N}$ (See Eq. 2.19). The diagonal elements of $\underline{\mathcal{L}}'$ are the eigenvalues $\epsilon_n = \pm\hbar\omega_n/2$, with each eigenvalue corresponding to a an eigenvector $\boldsymbol{u}_n$ of the EOM. At this point, it is worth ensuring the proper ordering of our eigenvalues in ascending order.

3. Third, the $\delta(\omega - \omega_n)$ term in Eq. 3.1 must be replaced by a smooth function with broadening set by the energy resolution of the measurements involved. For

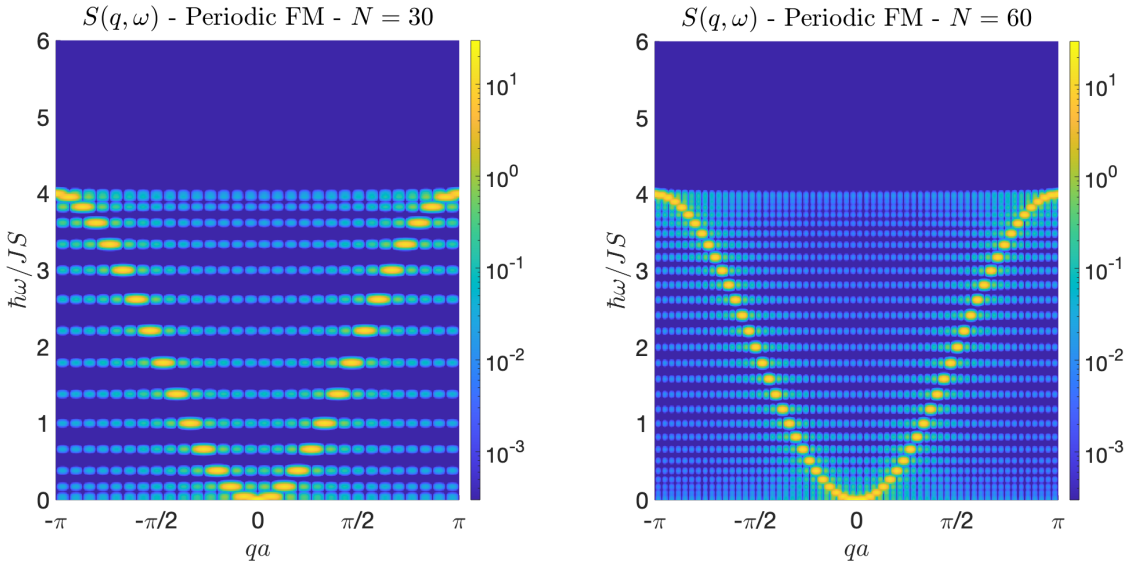

Figure 3.1: Scattering function of FM with periodic b.c.

INS the usual choice is

$$\frac{e^{-(\omega-\omega_n)^2/(2\Delta^2)}}{\sqrt{2\pi\Delta^2}} \tag{3.2}$$

with width proportional to the energy resolution Δ. In INS Δ is typically on the order of meV. As we are not concerned with exact physical quantities, we set $\Delta = 0.02$ for ease of plotting (again, we are using reduced units, so this does *not* correspond to units of meV).

4. Finally, we evaluate Eq. 3.1, and plot a heat map of the resulting spectrum for $\boldsymbol{q}\ vs.\ \omega$, using a log scale for the spectral weight.

3.1 FM with Periodic Boundary Conditions

The evaluation of $S_{x,x}(\boldsymbol{q},\omega)$ for the periodic FM serves two primary purposes. First, it allows us to compare our results to previous works, serving as an essential check to ensure our method of evaluating $S_{x,x}(\boldsymbol{q},\omega)$ is valid. Second, it serves as a reference point for us to compare our finite-size results. Our results are shown in Fig. 3.1. There we see that the curve of $S_{x,x}(\boldsymbol{q},\omega)$, for the periodic case, follows the $\sin(qa)^2$ dispersion discussed in chapter 1 . We see in Fig. 3.1 that as we increase N, $S_{x,x}(\boldsymbol{q},\omega)$ tends towards the bulk case.

The primary difference between the finite and the infinite cases is the discretized scattering lobes of the finite case. For the periodic case, there are $N/2+1$ lobes. The lobe width on the ω axis is dictated by Δ, while the number of spins, N, dictates the width in qa. Each discrete value of ω corresponds to several degenerate eigenstates.

3.1.1 Investigating the Eigenvectors

Understanding the physics behind the effects of anisotropy on $S_{xx}(q,\omega)$ is best achieved by studying the effects of anisotropy on the eigenstates of the system. The eigenvectors $\boldsymbol{u}_n$ of Eq. 2.21 characterize the eigenstates of the EOM, and have the form

$$\boldsymbol{u}_n = \left(\hat{a}_1(0), \hat{a}_2(0), \ldots, \hat{a}_N(0) | \hat{a}_1^\dagger(0), \hat{a}_2^\dagger(0), \ldots, \hat{a}_N^\dagger(0)\right). \tag{3.3}$$

We may represent the *energy* eigenstates of the system using the expectation value for the spin operator,

$$\langle \hat{S}_i^x(t=0)\rangle = \langle n| \frac{1}{\sqrt{2}} \left(\hat{a}_i^\dagger(0) + \hat{a}_i(0)\right) |n\rangle \text{ for } i = 1, \ldots, N. \tag{3.4}$$

From this representation we can construct the vector,

$$\langle \hat{\boldsymbol{S}}^x(t=0)\rangle = \left(\langle \hat{S}_1^x(t=0)\rangle, \langle \hat{S}_2^x(t=0)\rangle, \ldots, \langle \hat{S}_N^x(t=0)\rangle\right), \tag{3.5}$$

which describes the spatial form of the SW as shown in Fig 1.3.

We look at several of these vectors for the FM with periodic b.c. in Fig. 3.2 for a chain with $N = 10$ spins. The points correspond to the values of $\langle \hat{\boldsymbol{S}}_i^{\,x}(t=0)\rangle$ for $i = 1, \ldots, N$, while the curves are sinusoidals fitted to the points. Fig. 3.2 (a) shows the degenerate eigenvector of the highest energy state, ω_N. For each energy eigenvalue $\hbar\omega_n$ of the FM system, there are at least two corresponding eigenvectors; one with non-zero values of $\langle \hat{a}_i(0)\rangle$, and one with non-zero values of $\langle \hat{a}_i^\dagger(0)\rangle$, corresponding to $+\epsilon_n$ and $-\epsilon_n$, respectively. Fig. 3.2 (b) shows the degeneracy of the periodic FM, which has two degenerate eigenvectors corresponding to each ω_n for $n \neq 0, N$. Noticing that each eigenvector in Fig. 3.2(b) is $\pi/2$ out of phase with the other, it is evident why the ω_N and ω_0 modes are non-degenerate, while the remainder of the modes are two-fold degenerate.

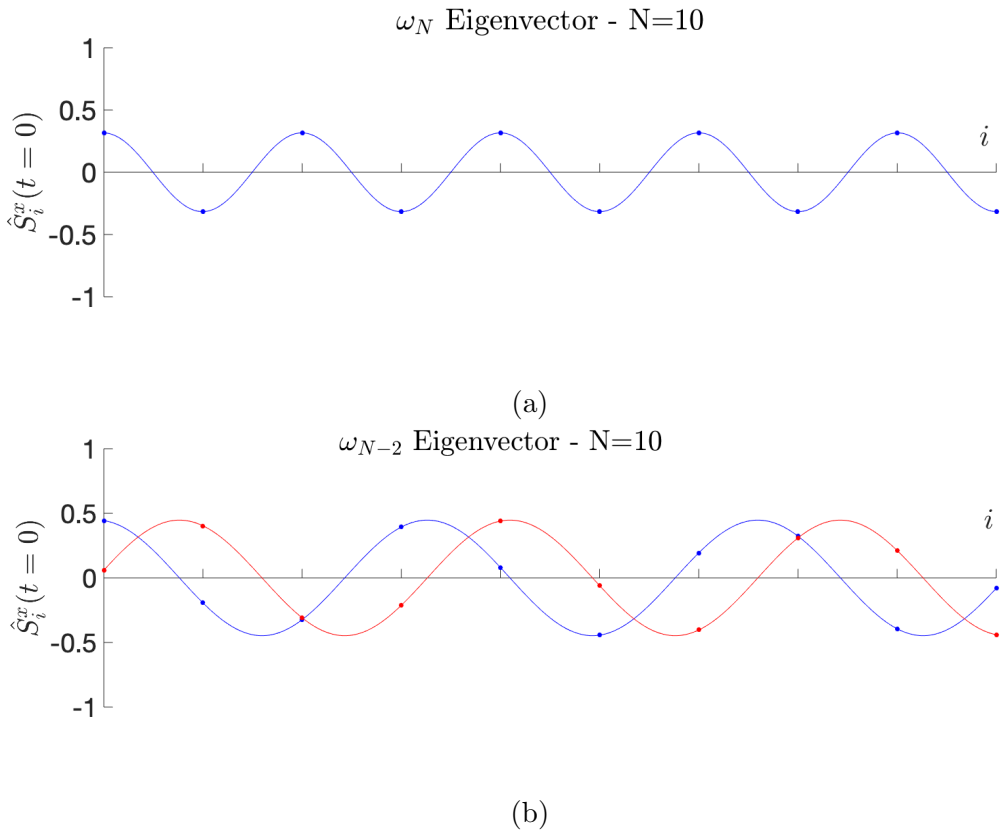

Figure 3.2: Eigenvectors of the periodic FM. (a) shows the non-degenerate ω_N mode, (b) shows the two-fold degenerate ω_{N-2} mode.

3.1.2 Investigating the Harmonics

One of the features of Fig 3.1 we wish to investigate is the presence of off-peak harmonics, and whether or not we should expect to see them in experiments. For simplicity, we will look at the ω_0 mode. We know,

$$\langle 0|\, \hat{a}_{i0,}\, |0\rangle = 1/\sqrt{N} \text{ and } \langle 0|\, \hat{a}^{\dagger}_{i,0}\, |0\rangle = 1/\sqrt{N} \text{ for } i = 1, \ldots, N. \tag{3.6}$$

From this and Eq. 2.30, we get $X_1(i,0)X_2(j,0) = 1/N \;\forall\; i,j$. Eq. 2.38 then reduces to

$$S_{x,x}(q,0) = \frac{\sigma S}{2N^2} \sum_{i,j} e^{-iq\cdot(R_i - R_j)} = \frac{\sigma S}{2N^2} \sum_{i,j} e^{-iqa(i-j)}, \tag{3.7}$$

where we have let $\sigma = (n_B(\omega_n) + 1)\delta(\omega - \omega_n)$ as we are holding ω constant for this analysis. When $N \to \infty$ (Fig. 3.3(a)), Eq. 3.7 becomes proportional to $\delta(qa)$, a statement of momentum conservation for the $\omega = 0$ excitation. For finite N, it contains the usual higher harmonics associated to the oscillatory approximation to the delta function. Expanding the sum in Eq. 3.7, we get,

$$S_{x,x}(q,0) = \frac{\sigma S}{N^2}\left[\frac{N}{2} + (N-1)\cos(qa) + (N-2)\cos(2qa) + \ldots + \cos((N-1)qa)\right]. \tag{3.8}$$

This analytic result is plotted along with our numerical results in Fig. 3.3(b). We can look at the slightly more complicated ω_N mode for which,

$$\langle N|\, \hat{a}_{i0,}\, |N\rangle = (-1)^i/\sqrt{N} \text{ and } \langle N|\, \hat{a}^{\dagger}_{i,0}\, |N\rangle = (-1)^i/\sqrt{N} \text{ for } i = 1, \ldots, N. \tag{3.9}$$

Repeating the same procedure as we preformed for $|0\rangle$, we get,

$$\begin{aligned} S_{x,x}(q,\omega_N) =& \frac{\sigma S}{N^2}\big[\frac{N}{2} - (N-1)\cos(qa) + (N-2)\cos(2qa) - (N-3)\cos(3qa) \\ &+ \ldots + \cos((N-1)qa)\big], \end{aligned} \tag{3.10}$$

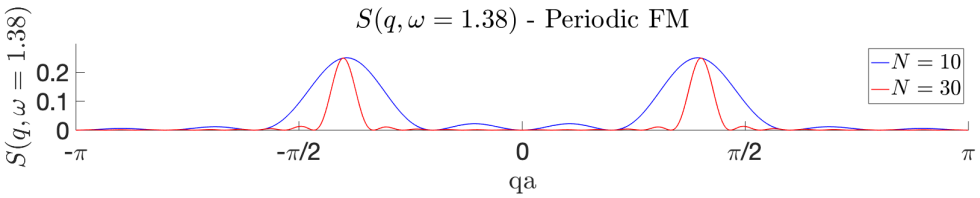

(a) Scattering function harmonics - Size dependence

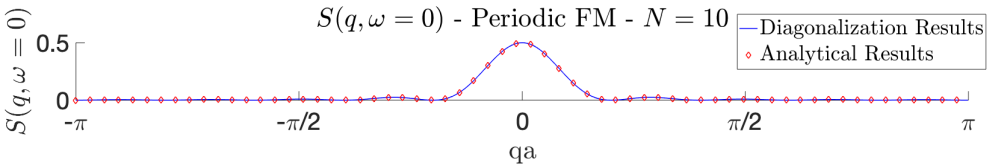

(b) Scattering function harmonics - Low energy ($\omega = 0$) excitation

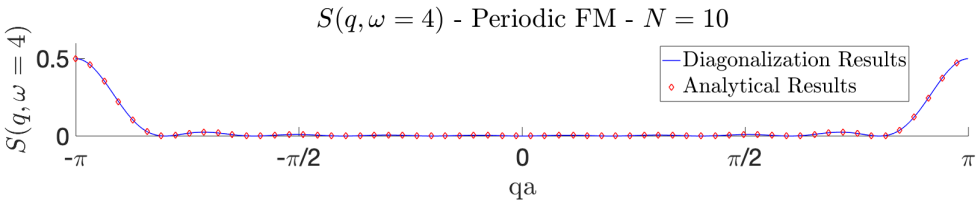

(c) Scattering function harmonics - High energy ($\omega = 4$) excitation

Figure 3.3: Harmonics in periodic FM

which, again, matches our results perfectly, as can be seen in Fig. 3.3 (c).

These results show that the series of harmonics appearing in Fig. 3.3 arise from momentum conservation in a finite system of N sites. These harmonics are physical and can be detected should the experimental resolution be high enough. If the experiment is unable to resolve the harmonics, they will appear as broadening of the primary peak [10].

3.2 FM with Open Boundary Conditions and Edge Anisotropy

The FM with open boundary conditions and $K = 0$ and $K_S = 0$ is shown in Fig. 3.4, while the FM with open boundary conditions and $K = 0.4$ and $K_s = 0$ is shown in Fig. 3.5 (a). Two major features distinguish the case in Fig. 3.4 from the periodic b.c. of Fig. 3.1. First, there are N distinct values of $\hbar\omega/JS$, as opposed to the $N/2+1$ values in the periodic case. The reason why the two-fold degeneracy is lifted is because the $\pi/2$ out of phase eigenvectors from Fig. 3.2 (b) are no longer degenerate in the open b.c. case (their energies split). Secondly, we see that the harmonics shift

away from $qa = 0$. Fig. 3.5(a) shows that as expected, the effect of bulk anisotropy on a FM system is to shift the SW spectra uniformly to higher energies, opening a *anisotropy gap* in the bulk SW spectra.

In Figs. 3.5(a) and 3.5(b), we can see that EP edge anisotropy leads to a localized mode with frequency smaller than the lowest bulk SW mode, i.e. within the anisotropy gap. As we lower K_s, the frequency of the mode lies right inside the gap, with spin oscillations localized at the edge of the chain. We will refer to these modes as acoustic edge modes. In Figs. 3.6 and 3.7, we see that the origin of the edge modes is the distortion of the low energy modes. Even for low values of $|K_s|$, these modes are significantly distorted from their sinusoidal form, leading to the broadening of their spectral weights. While there is a mild distortion of the other modes, it takes the form of small changes in wavelength and phase, resulting only in the shift in harmonics, as seen in Figs. of 3.5. Fig. 3.5(d) shows that EA edge anisotropy gives rise to an edge mode at high frequency – we call this the optical edge mode.

Figs. 3.6, 3.7 and 3.8 explore the nature of the edge modes, and their subsequent effect on the scattering function. Fig. 3.6 shows the rise of the acoustic edge modes due to EP edge anisotropy. Fig. 3.6 (a) shows the lowest-frequency ω_0 mode, which corresponds to a uniform precession about the axis of bulk anisotropy (z-axis in our case). It shows the distortion of the uniform ω_0 mode, and the subsequent broadening of the scattering function. The other localized edge mode is ω_1, which is associated to wavevector $|q| \approx 2\pi/N$. Its frequency is quite close to ω_0, but it has quite different eigenvectors in that it corresponds to antisymmetric oscillations in space, see Fig 3.7.

Unlike the bulk modes, for both edge modes, the magnitude of the precession cones decreases monotonically from the largest value at the edge, to the smallest value at the centre. The decrease in magnitude follows an exponential decay.

Fig. 3.8 shows additional special cases for the FM edge modes. Figs. 3.8 (a)-(d) show the effects of different values of K_s on each edge. We see that this destroys the symmetric and antisymmetric modes, leaving oscillations at only one edge of the chain. Note how the scattering function no longer exhibits higher harmonics as a function of q, due to the complete destruction of translation symmetry.

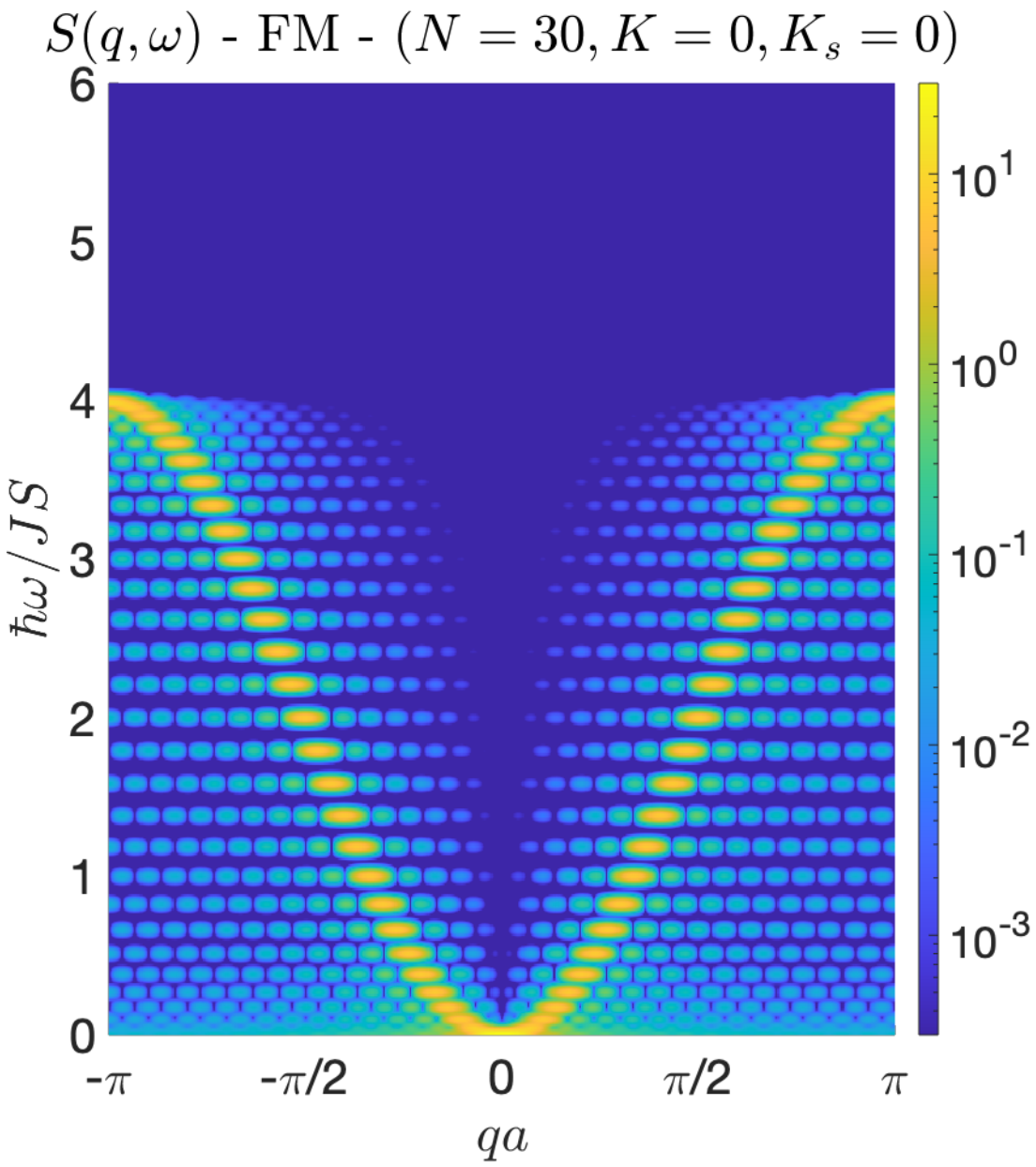

Figure 3.4: Scattering function of finite FM with open b.c. for $K_s = 0$ and with $K = 0.0$.

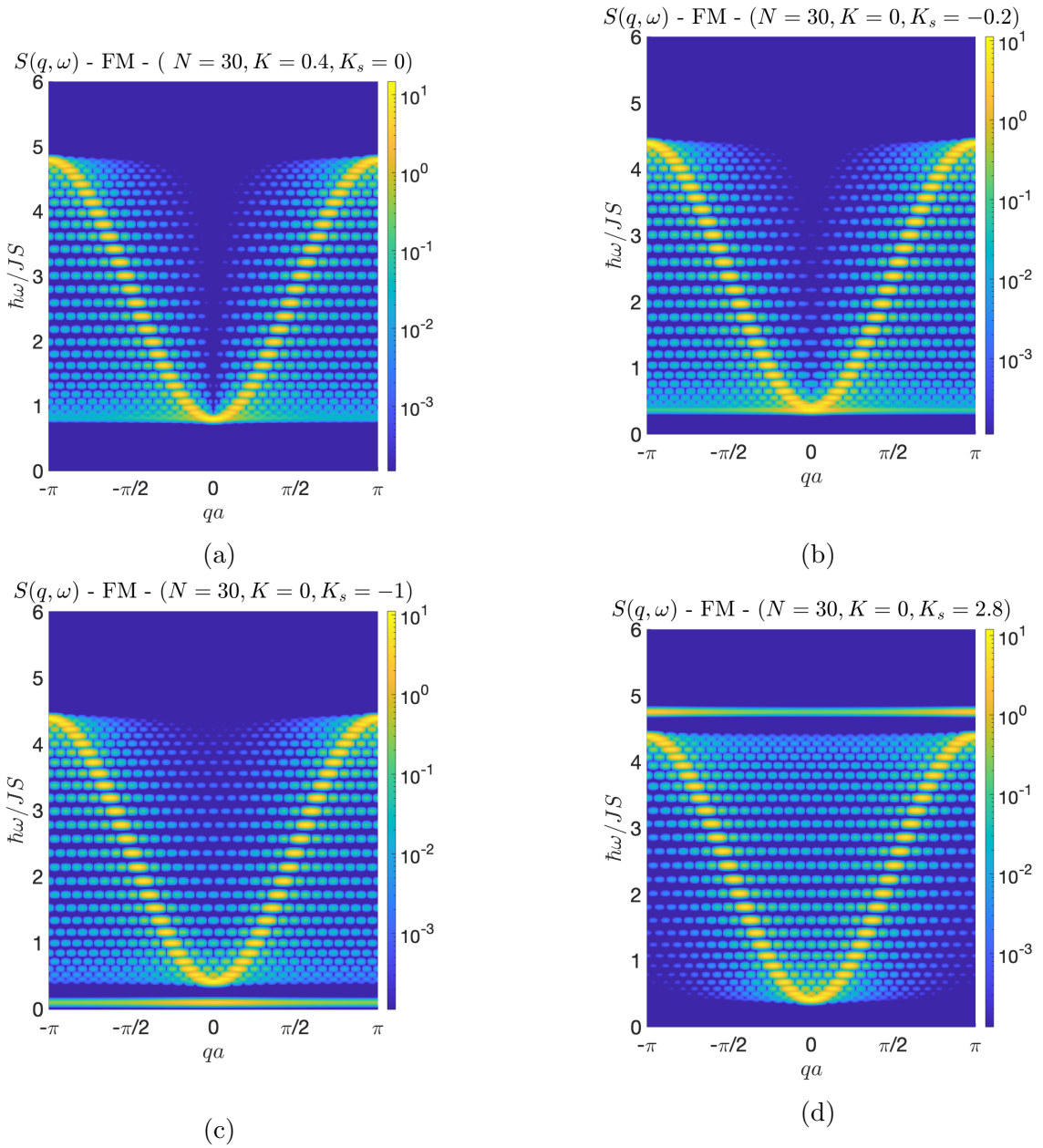

Figure 3.5: Scattering function of finite FM chain for several values of K_s, with a fixed $K = 0.4$ EA bulk anisotropy.

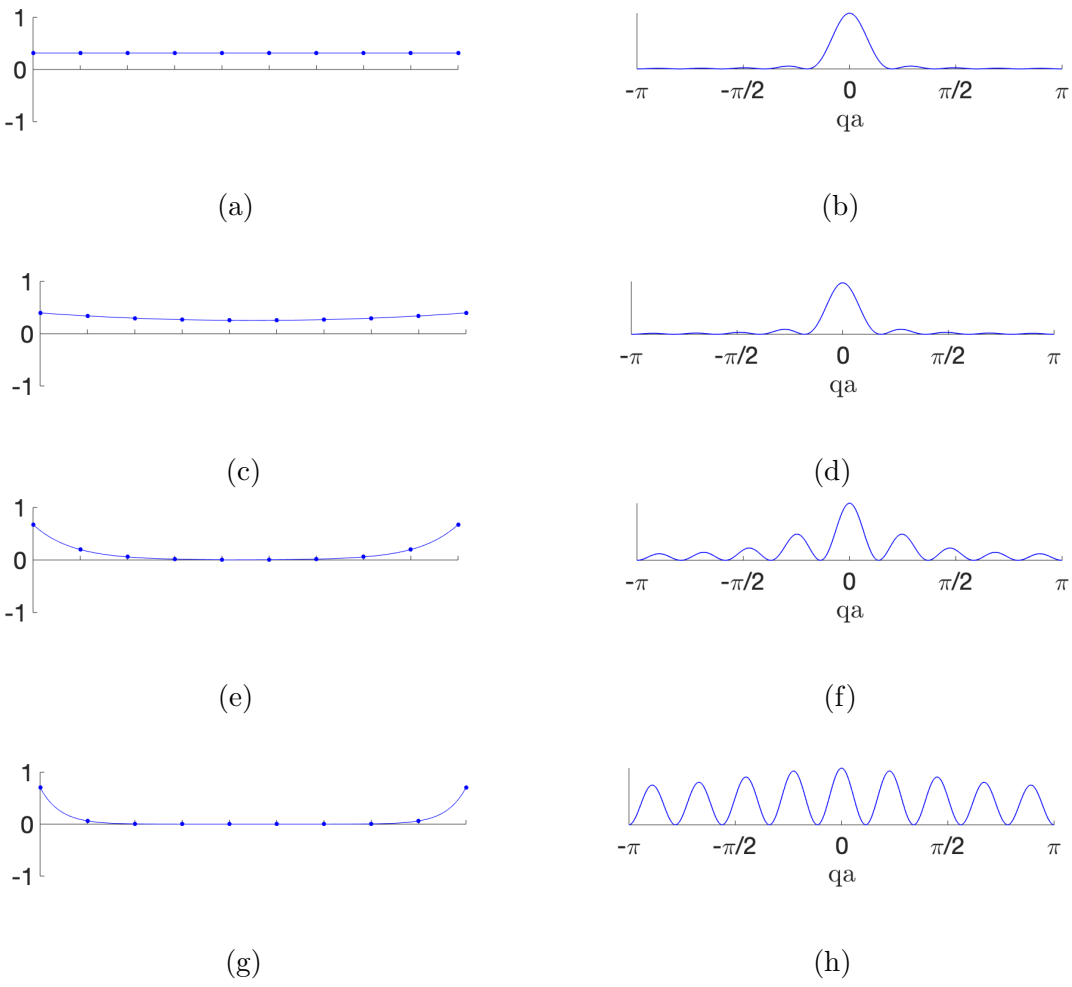

Figure 3.6: The rise of lowest frequency ω_0 symmetric acoustic edge modes in FM for decreasing values of K_s. (a),(b) have $K_s = 0$, (c),(d) have $K_s = -0.2$, (e),(f) have $K_s = -1$, (g),(h) have $K_s = -10$. In all cases $K = 0.4$. Minimal labelling has been included for clarity. See Figs. 3.2 and 3.3 for further description of interpretation.

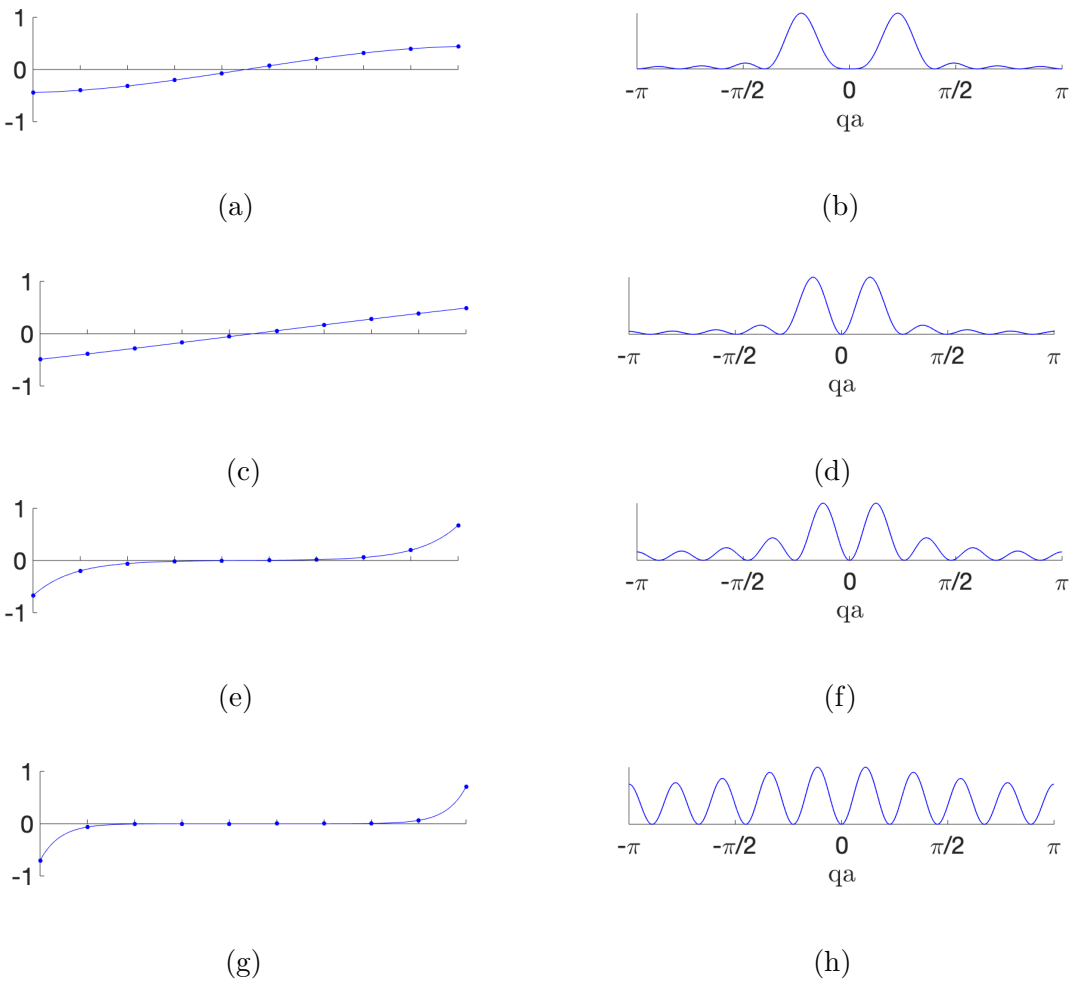

Figure 3.7: The rise of the second lowest frequency edge mode ω_1, associated to $|q| \approx 2\pi/N$ in a FM, for decreasing values of K_s. (a),(b) have $K_s = 0$, (c),(d) have $K_s = -0.2$, (e),(f) have $K_s = -1$, (g),(h) have $K_s = -10$. In all cases $K = 0.4$. Minimal labelling has been included for clarity. See Figs. 3.2 and 3.3 for further description of interpretation.

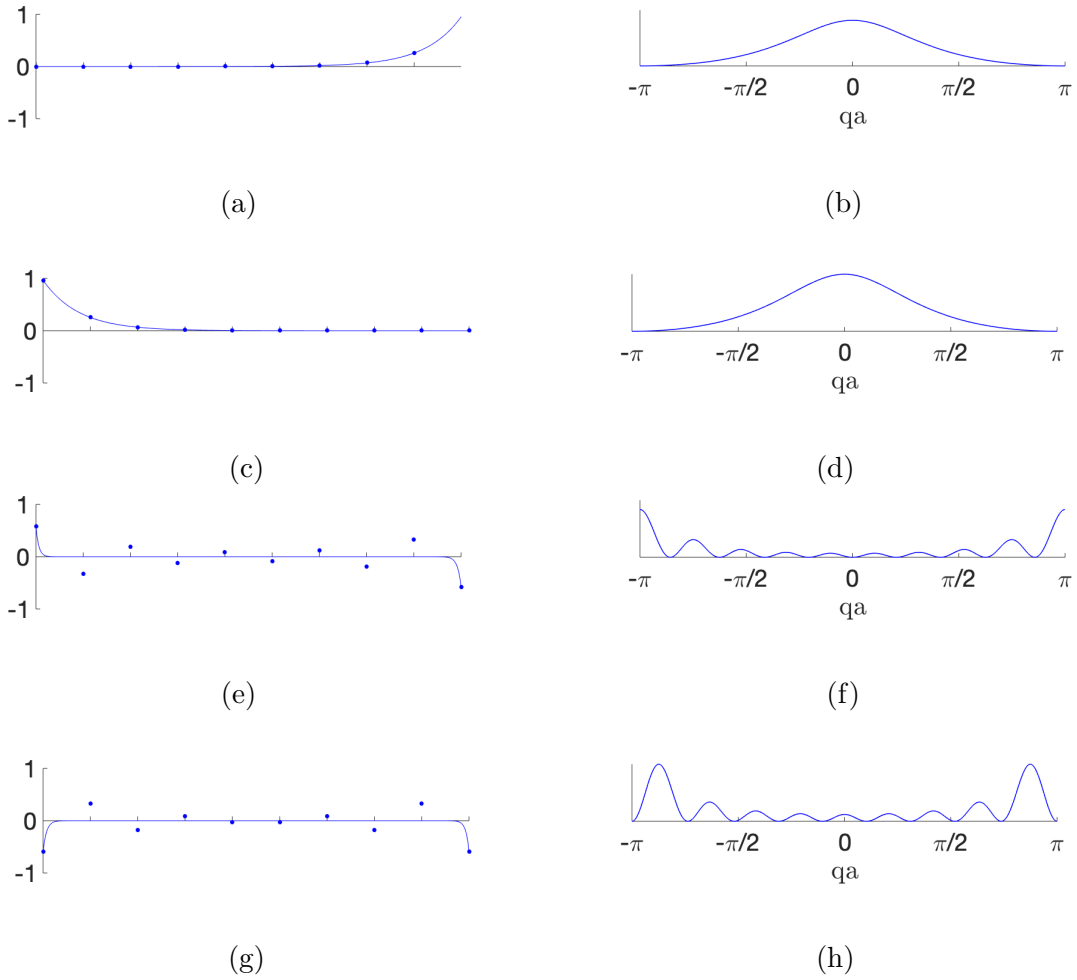

Figure 3.8: Here we show some special cases of the FM edge modes. Figs. (a)-(d) show the effects of different values of K_s at each edge on the low-frequency acoustic edge modes ((a) and (b) correspond to ω_0, while (c) and (d) correspond to ω_1), with $K_{s,1} = -10$ and $K_{s,N} = -6$. Figs. (e)-(h) show the symmetric and asymmetric high-frequncy (ω_N and ω_{N-1}) optical edge modes for $K_s = 2.8$. In all cases $K = 0.4$. Minimal labelling has been included for clarity. See Figs. 3.2 and 3.3 for further description of interpretation.

Figs. 3.8 (e)-(h) show the high energy optical edge modes due to EA edge anisotropy $K_s = 2.8$. The optical mode has each precession cone 180° out-of-phase with its neighbour. The magnitude of the oscillations still decreases monotonically towards the centre with exponential decay.

Chapter 4

Numerical Results for the Antiferromagnetic Chain

4.1 AFM with Periodic Boundary Conditions

$S_{xx}(\vec{q},\omega)$ for the periodic AFM case is shown in figure 4.1 for $N = 30$. As we can see in Fig. 4.1 (a), the shape of $S_{xx}(\vec{q},\omega)$ matches the known $|\sin(qa)|$ dispersion of an infinite AFM chain. Similar to the FM case, $S_{xx}(\vec{q},\omega)$ becomes discretized at finite sizes. For the periodic case, the eigenstates are highly degenerate with $N/4+1$ distinct values of $\hbar\omega/JS$. When $mod(N,4) \neq 0$, there are $(N - mod(N,4))/4 + 1$ distinct values of $\hbar\omega/JS$, with the non-ω_N/ω_0 modes being 4-fold degenerate. The eigenvectors of the AFM case are slightly more complicated than those of the FM case, as we can see in Fig. 4.2. The increase in complexity is due to each sub-lattice having a partially independent waveform. For the periodic case, the dispersion of lattices A and B are degenerate, explaining one part of the degeneracy we see.

As we saw in the ferromagnetic case, out-of-phase pairs for each set of eigenvectors cause further degeneracy. Fig. 4.1 shows that bulk EA anisotropy no longer causes a uniform increase in the energy of the SW modes. While the energy of all SW modes do increase, it is not uniform, which results in an increase in the density of states, as the low ω states are more affected than the high ω states.

4.2 AFM with Open Boundary Conditions and Edge Anisotropy

In Fig. 4.3 (a), we can see the introduction of open boundary conditions eliminates the out-of-phase degeneracies as it did in the FM case. This leaves us with $N/2$

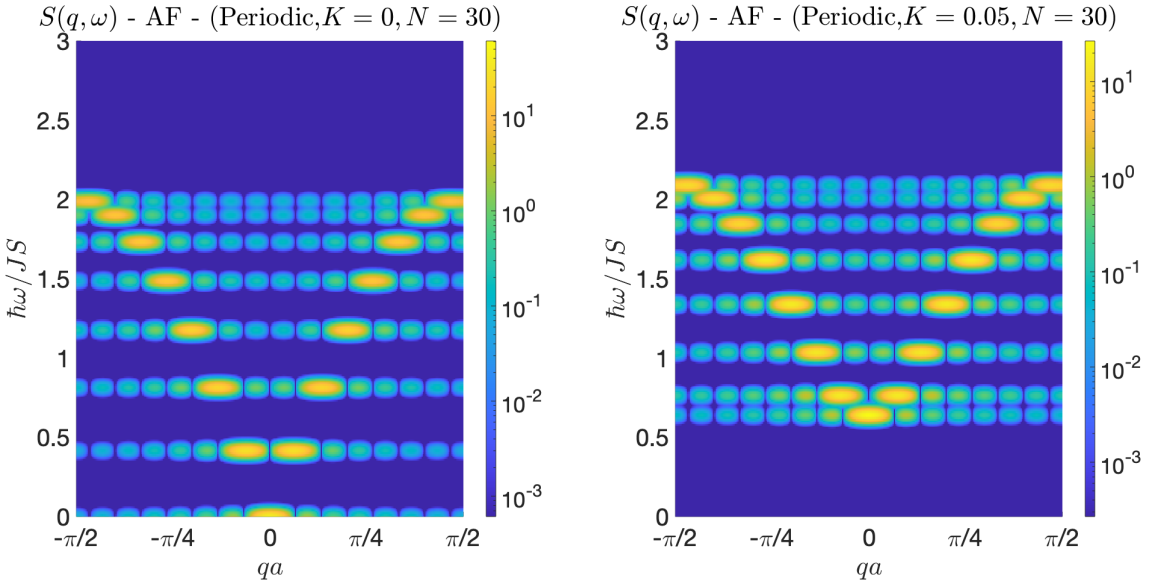

Figure 4.1: Scattering function of periodic AFM. (a) Zero magnetic anisotropy and (b) easy-axis bulk anisotropy with K=0.05.

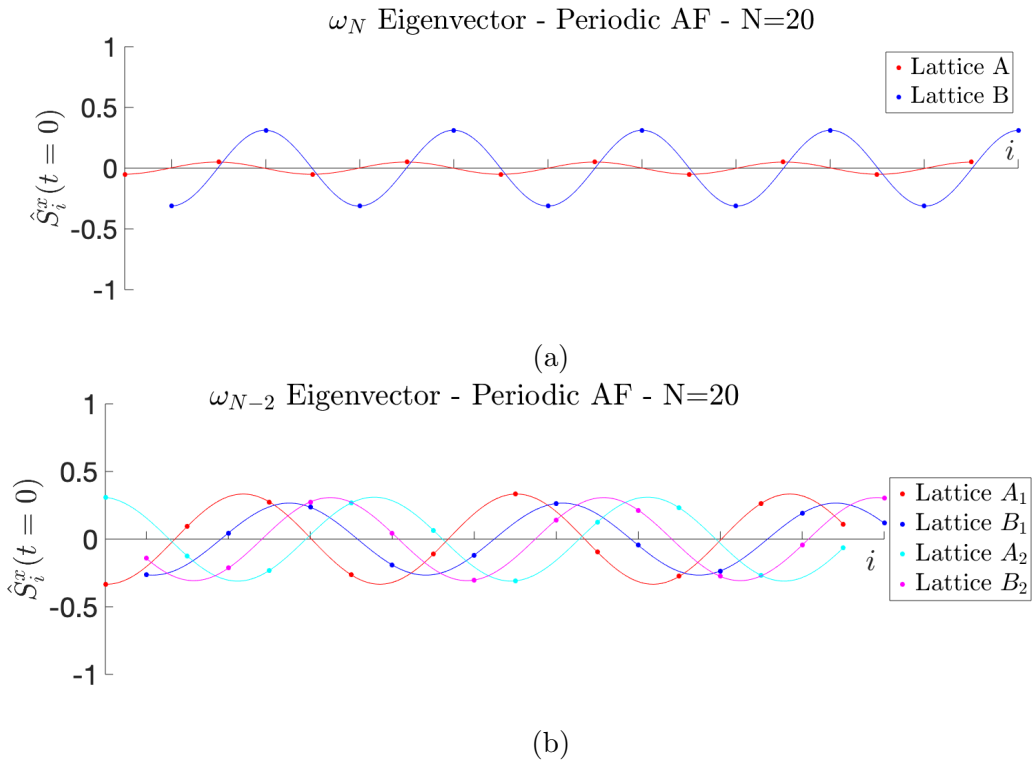

Figure 4.2: Eigenvectors of periodic AFM. Fig. (a) shows eigenvectors of two-fold degenerate ω_N mode, Fig. (b) shows eigenvectors of four-fold degenerate ω_{N-2} mode.

distinct values of $\hbar\omega/JS$, as sub-lattices A and B still have degenerate dispersions. We do not see the shift of the harmonics to high qa that we saw in the FM case. Furthermore, we see that the introduction of open boundary conditions gives rise to a broadened low energy mode in the presence of an EA bulk anisotropy. It turns out that this mode is indeed an acoustic edge mode, as we can see in Fig. 4.4 (b). In Figs. 4.3 (b)-(d), we see that the energy of the acoustic mode decreases with EP edge anisotropy, and increases with EA edge anisotropy. This behaviour is the opposite of the FM case, where EA edge anisotropy decreases the acoustic mode's energy. As can be seen in Figs. 4.4 (g) and (h), for a specific range of EA edge anisotropy, the acoustic mode disappears, reappearing as an optical mode for large K_s as can be seen in Fig. 4.3 (d). We do see the same shift of the harmonics towards lower qa as we increase K_s, as we saw in the FM case.

Figs. 4.4 (a)-(d) show the effects of edge anisotropy on the acoustic modes of the AFM chain. While the magnitudes of the precession cones no longer decrease monotonically towards the centre, as in the FM case, the magnitudes of the precession cones within a given lattice *do* decrease monotonically towards the centre, with exponential decay. We see the edge modes are no longer even and odd under parity symmetry as in the FM case, instead behaving like the FM case with asymmetrical values of K_s at either edge. We still see broadening of the scattering function; however, it is significantly less pronounced than in the FM case, and does not show harmonics.

Fig. 4.5 shows the acoustic mode behaviour of the uncompensated $N = 21$ case. Here lattice A has 11 spins while lattice B only has 10 spins. In contrast to the compensated case, the uncompensated case has inversion symmetry about the spin in the middle of the chain. It also has lattice A being pinned at either end by the edge anisotropy. Here we see the acoustic mode is symmetric, unlike the acoustic mode in the compensated case. The uncompensated case behaves like a compensated case in response to edge anisotropy, with a slightly more significant broadening of the scattering function and demonstration of harmonics. The uncompensated case also results in the A and B lattice SWs no longer being degenerate; however, the energy gap between the corresponding SWs remains small.

Fig. 4.6 shows the optical modes of the AFM chain. The optical modes arise as

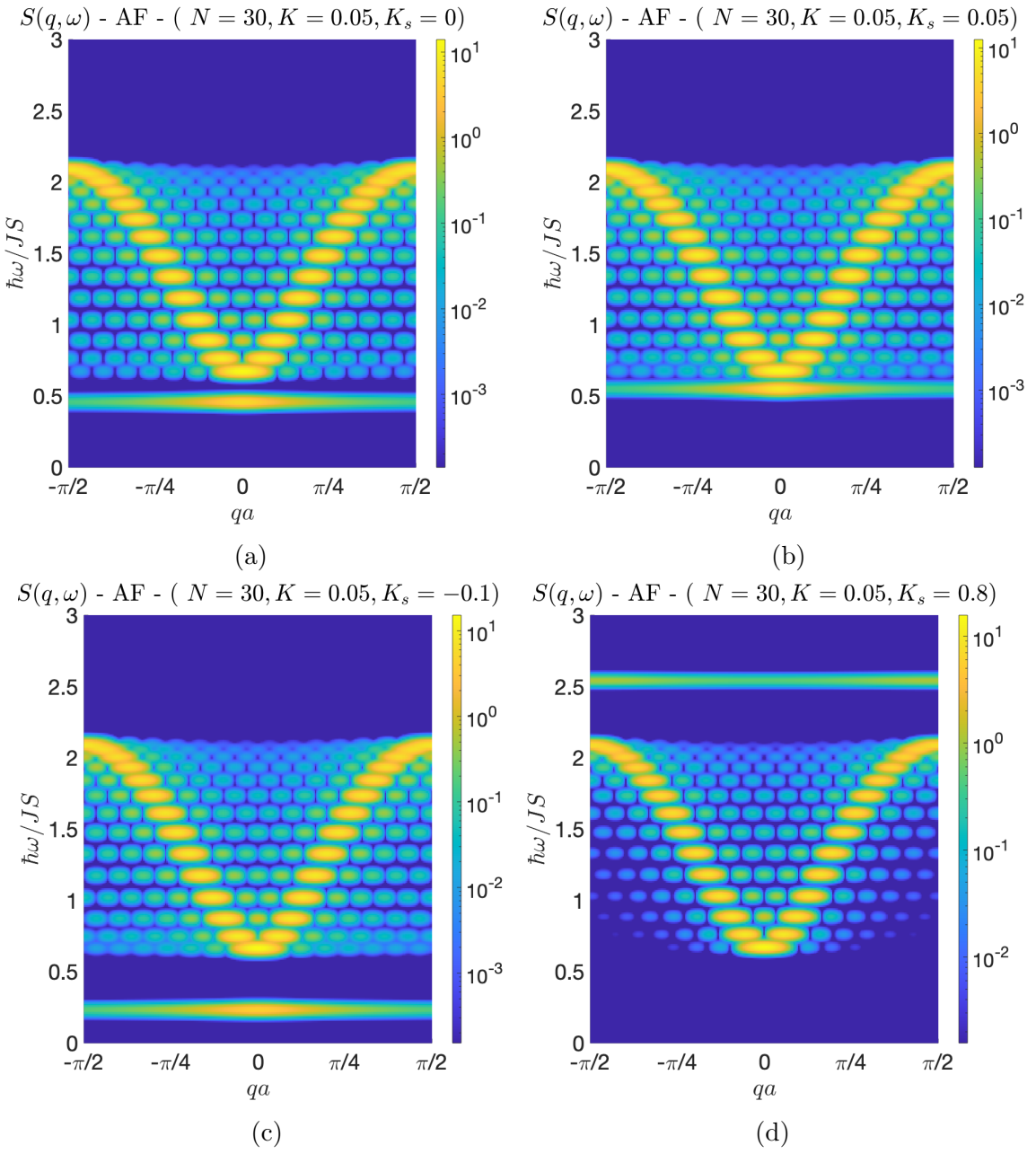

Figure 4.3: Scattering function of finite AFM chain with open boundary conditions for several values of K_s, with a fixed $K = 0.05$ EA bulk anisotropy.

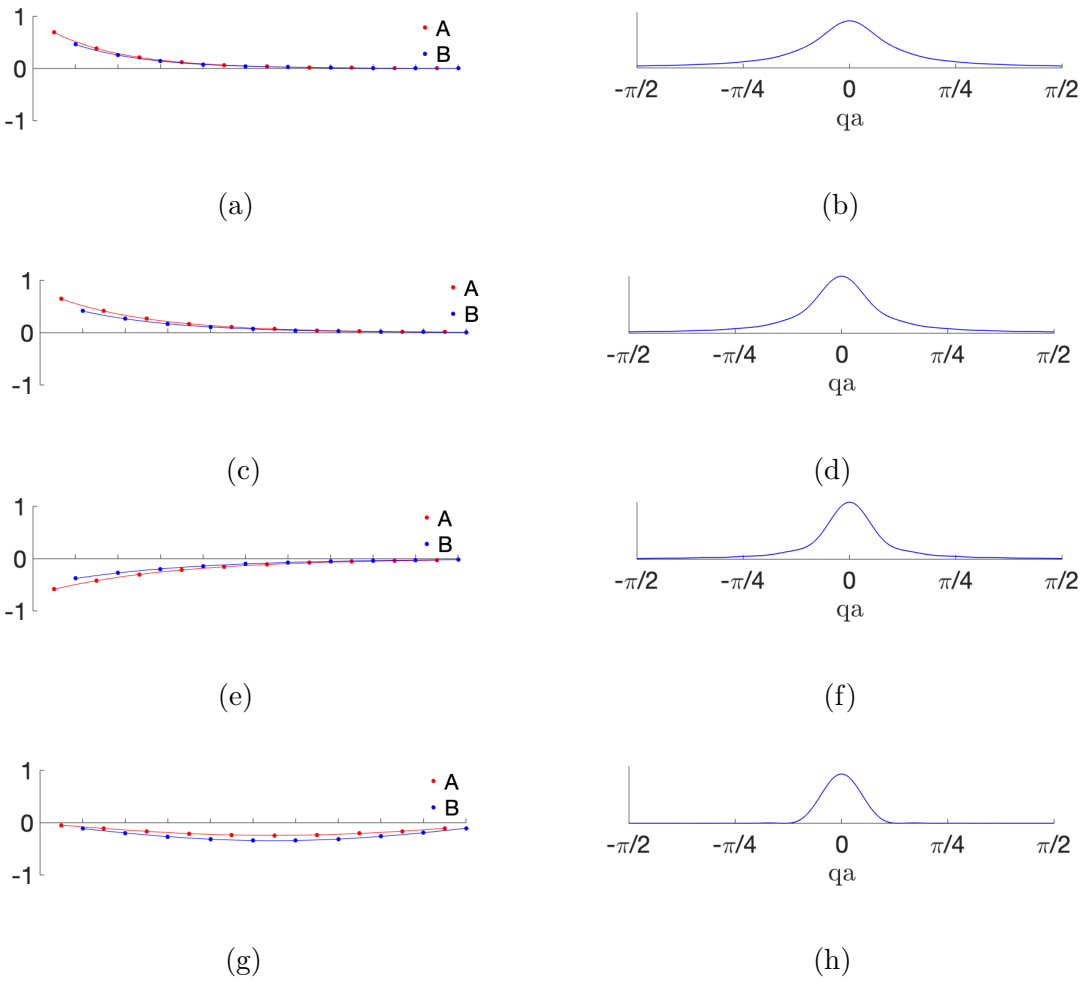

Figure 4.4: Eigenvectors of the compensated AFM low ω acoustic edge modes, for several values of K_s and with $K = 0.05$. Figs. (a) - (f) show the acoustic modes for $K_s = -0.1, 0$ and 0.05, while Figs. (g) and (h) show the lowest energy mode for $K_s = 0.3$, which is not an edge mode. In all cases $K = 0.05$ and $N = 20$. Minimal labelling has been included for clarity. See Figs. 4.2 and 3.3 for further description of interpretation.

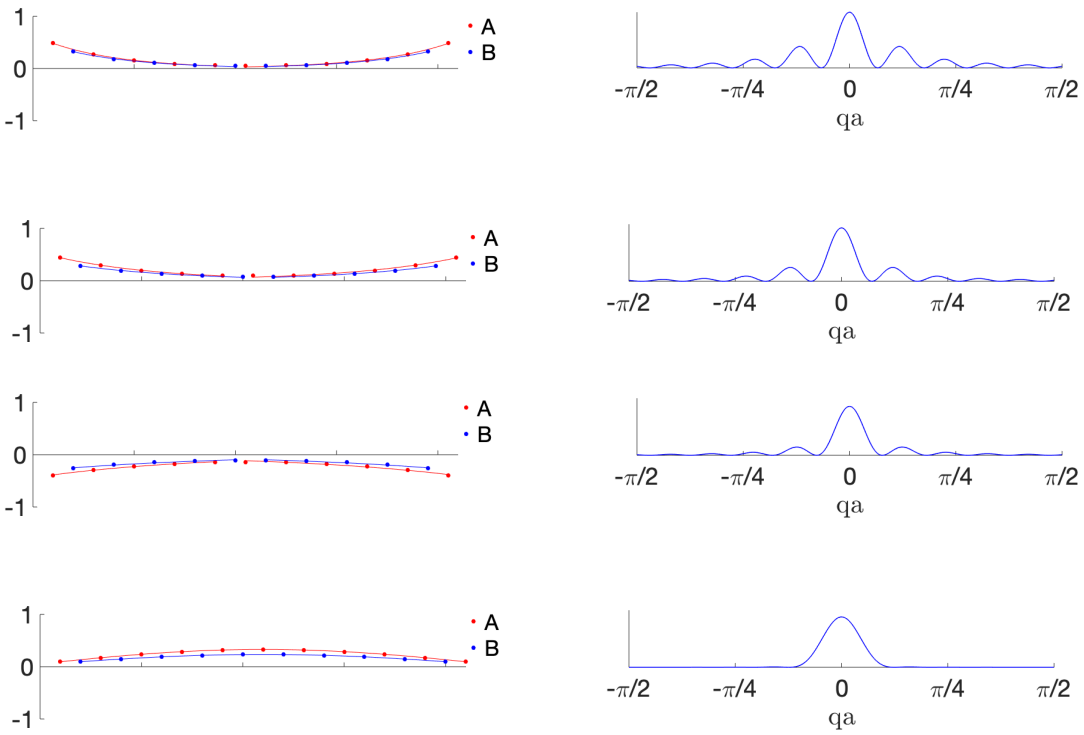

Figure 4.5: Eigenvectors of the uncompensated AFM low ω acoustic edge modes, for several values of K_s and with $K = 0.05$. Figs. (a) - (f) show the acoustic modes for $K_s = -0.1, 0$ and 0.05, while Figs. (g) and (h) show the lowest energy mode for $K_s = 0.3$, which is not an edge mode. In all cases $K = 0.05$ and $N = 21$. Minimal labelling has been included for clarity. See Figs. 4.2 and 3.3 for further description of interpretation.

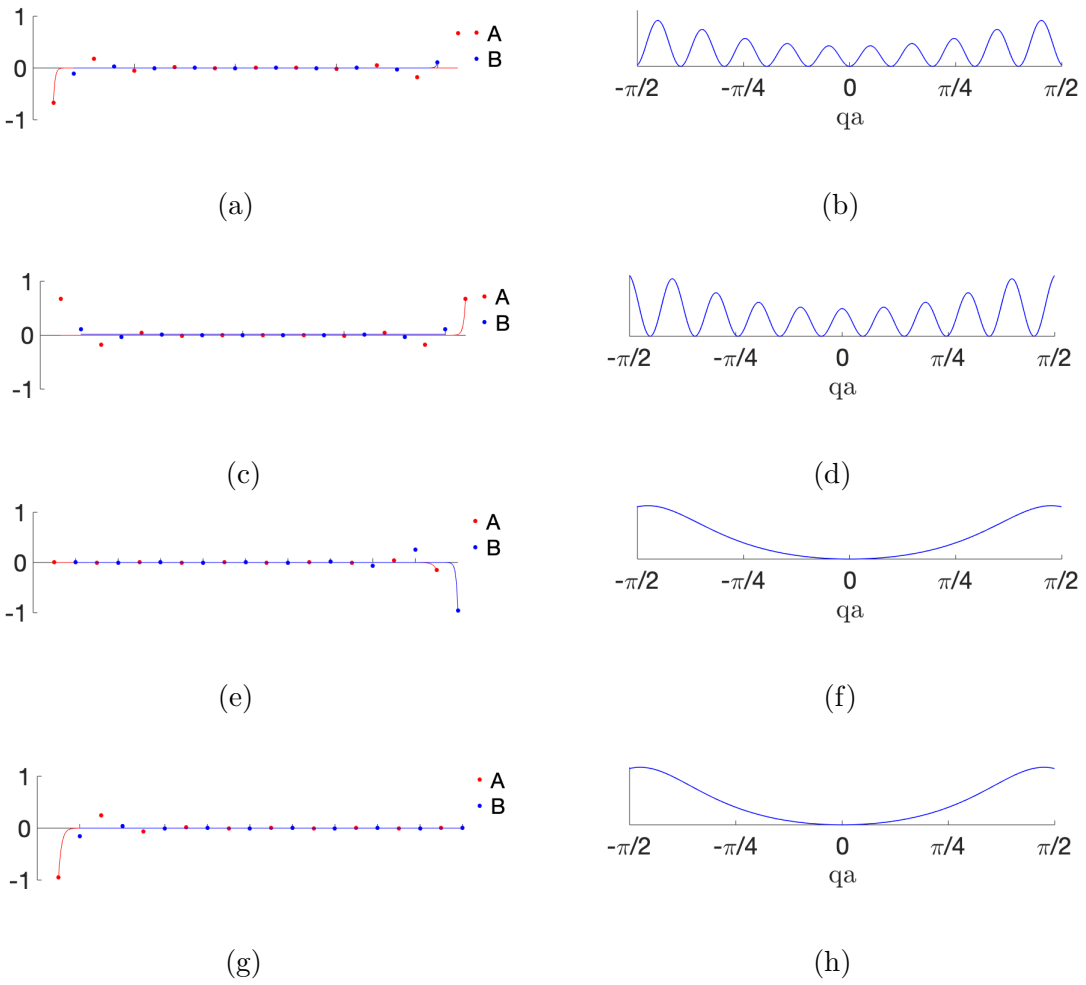

Figure 4.6: Eigenvectors of the AFM high ω optical edge modes, with $K = 0.05$ and $K_s = 0.8$. Figs. (a) - (d) show the uncompensated case ($N = 21$), while Figs. (e) - (h) show the compensated case ($N = 20$).

a result of large EA anisotropy. We see that sublattices A and B individually exhibit the same behaviour as the FM case's optical modes, with the precession cone of each spin site of the sublattice being 180° out of phase with the neighbouring spins in the sublattice, with magnitudes decreasing exponentially towards the centre. The scattering function of the compensated case in Figs. 4.6 (f)-(h) do not show harmonics, while the uncompensated case in Figs. 4.6 (a)-(d) do show harmonics. This behaviour is consistent with the behaviour we saw in the compensated/uncompensated acoustic modes.

Chapter 5

Discussions and Conclusions

5.1 Analysis of FM results

The first task in analyzing our work is to compare it to previous work. This both validates our approach, as well as hopefully serves as a tool for extrapolating our results to three dimensions. Figure 5.1(a) shows $S_{xx}(q,\omega)$ when the formalism we used is applied to a bulk FM system. We see similar results to our own, with more intense scattering near $q = 0$ and $q = 2\pi$ due to an increased density in states. Figure 5.1(b) shows $S_{xx}(q,\omega)$ for an FCC nanoparticle. Here, similar to our results, we see a discretized spectra with broad peaks in q.

Furthermore, in figure 5.1(b), we see the presence of off-peak harmonics along q. These results provide a strong reference point for extrapolating our results to three dimensions. While the exact nature of the peaks is different in the three-dimensional case, the overall properties are much the same, suggesting our 1D results may provide valuable insights into the nature of INS of nanoparticle systems.

The emergence of the acoustic and optical modes as a result of edge anisotropy is supported by previous works [11]. The effects of edge anisotropy on the energy (frequency) of the excitations are shown in Fig. 5.2. We see that while EP edge anisotropy *increases* the energy (relative to the $K_s = 0$ case) of both the ground state and the first excited state, the increase in the ground state energy is greater, resulting in a *decrease* in excitation energy, i.e. $\hbar\omega_0' < \hbar\omega_0$. Similarly, we see that EA edge anisotropy *decreases* the energy of both ground and highest excited states. The decrease in energy of the ground state is greater, *increasing* excitation energy, i.e. $\hbar\omega_N'' > \hbar\omega_N$.

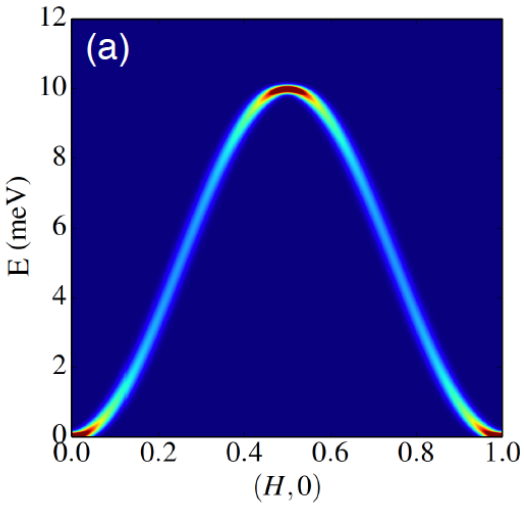

(a) $S(q,\omega)$ of bulk 2D square lattice FM. [1]

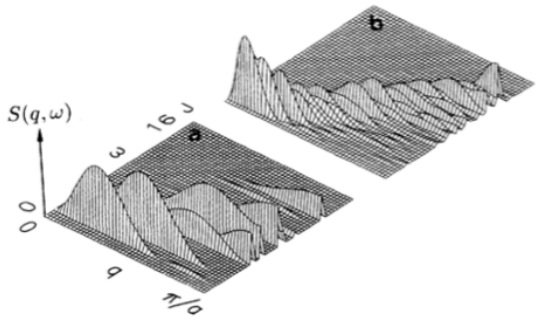

(b) $S(q,\omega)$ for FCC cluster along the (111) direction. (a) corresponds to N=55 (b) corresponds to N = 683 spins. [10]

Figure 5.1: Known $S(q,\omega)$ for FM cases

The behaviour seen in Fig. 5.2 is congruent with the behaviour seen in the eigenvectors in Figs. 3.6 and 3.8. In the case of EP edge anisotropy (Fig. 3.6) the energy of both ground and excited states are increased as the majority of the spin lies in the z-axis. The energy of the first excited state is then minimized by localizing the excitation to the edge spins, where the total anisotropy is $K + K_s$ is *lower* than the total anisotropy K for the bulk spins. The difference in anisotropy means the energy penalty for spins lying outside the z-axis is lower for the edge spins than the bulk spins.

For the EA edge anisotropy case, EA edge anisotropy lowers the ground and excited states' energy. However, now the total anisotropy at the edge spins is *higher* than that of the bulk spins. As we see in Fig. 3.8, localization of the spins to the edge in the optical mode reduces the change in energy of the highest excited state between $K_s = 0$ and $K_s > 0$ cases, resulting in $\hbar\omega''_N > \hbar\omega_N$, for large enough values of K_s.

Understanding the effects of edge anisotropy on the eigenvectors of the system, paired with the signature spectrums of the edge modes in Figs. 3.6, 3.7 and 3.8 should provide useful tools for the analysis of SWs in nanoscale magnetic systems.

5.2 Analysis of AFM results

While less work has been done in the field of neutron scattering in finite AFM systems, we do have Fig. 5.3 which shows $S_{xx}(q, \omega)$ when a similar formalism to the one we used is applied to a bulk AFM system. Comparing our results from Fig. 4.1 for the periodic AFM, we see that our results have a similar form to those in Fig. 5.3, however, $S_{xx}(q, \omega)$ in Fig. 4.1 does not show the same dependence on q that is seen in Fig 5.3. This result suggests that finite size has an appreciable affect on the $\boldsymbol{q}$ dependance of $S_{xx}(q, \omega)$.

The first significant result of the AFM case is the emergence of acoustic modes due to finite size and a bulk EA anisotropy, without the presence of edge anisotropy. The physical interpretation of this behaviour is not readily evident. We know it is not due to asymmetry at the boundaries of the sublattices, as the acoustic modes still exist in the uncompensated case ($N/2 + 1$ spins in lattice A, and $N/2$ spins in lattice

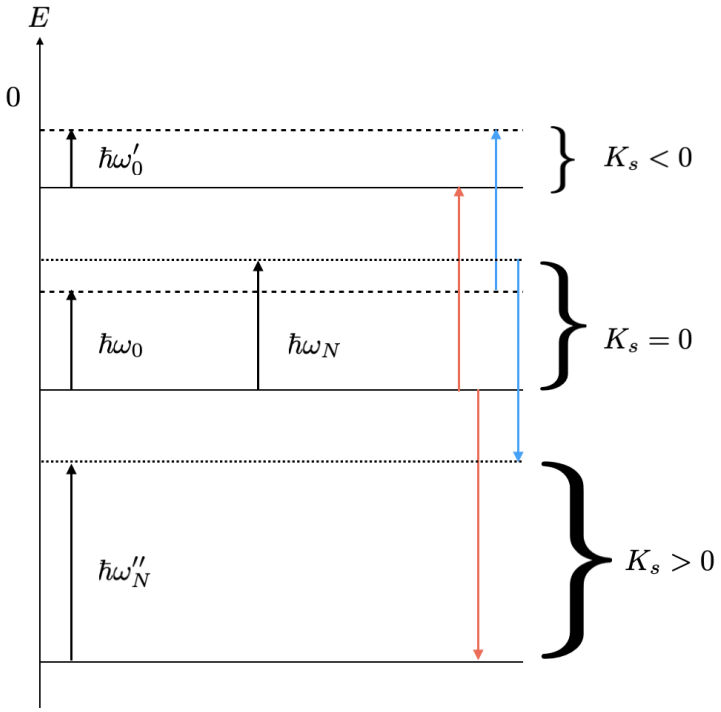

Figure 5.2: Effects of anisotropy on the energy (frequency) of spin configurations. Red arrows indicate change in ground state energy due to K_s, while blue arrows indicate change in energy of excited states due to K_s. In all cases we assume $K > 0$ (bulk EA anisotropy). Note: not to scale

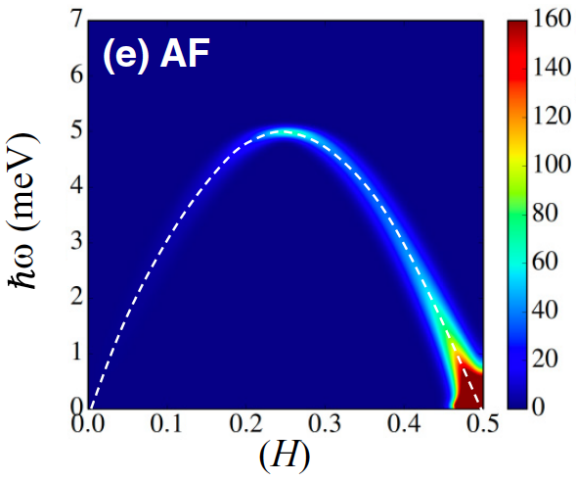

Figure 5.3: $S(q, \omega)$ of bulk 2D square lattice AFM. [1]

B). We can further rule out it being purely due to finite size effects, as the acoustic modes do not exist without the anisotropy. This result, should it translate to the 3D case, would be of particular significance as the existence of the edge mode does not require edge anisotropy.

Like the FM case, the energy and degree of localization of the edge mode are tuneable via the edge anisotropy. The compensated AFM is not symmetric under inversion in the centre of the chain, and as a result the edge modes are not parity even and odd like the FM case. As a result, the compensated AFM edge modes' behaviour parallels that of the FM case with asymmetric values of K_s. It then follows that the behaviour of the uncompensated AFM case parallels the behaviour of the FM case with symmetric values of K_s, with edge modes being even and odd with respect to space inversion at the centre. Similar to the FM case, EA edge anisotropy causes an increase in acoustic mode energy, while EP edge anisotropy causes a decrease in the acoustic mode energy. For high enough values of EA edge anisotropy, a high energy optical mode emerges.

5.3 Conclusions

Our work on evaluating the INS scattering function for 1D finite FM and AFM systems with bulk and edge anisotropies has shown the emergence of novel behaviour. In the FM case under the influence of EP edge anisotropy, we see the emergence of a low energy acoustic edge mode, as seen in studies of semi-infinite FM thin films [11]. In our finite case, the acoustic mode causes a significant broadening of the scattering peak in the low-energy states. We then show the emergence of a broad peaked optical edge mode due to large EA edge anisotropy. Similarities between our results and previous works on 3D cases suggest extrapolation of our results to physical systems is reasonable. Our results in the AFM case show the emergence of a broad peaked acoustic mode under the influence of bulk anisotropy and open boundary conditions. We show that the acoustic mode's energy is tunable through edge anisotropy, with a high energy optical mode emerging in the presence of large EA edge anisotropy.

We achieve these results by adapting the framework outlined by Fishman *et. Al.* [1] for evaluating the INS scattering function for bulk materials, the finite case, and

adding edge anisotropy terms. The framework boils down to determining the eigenstates of the system after a Holstein-Primakoff transformation of the Hamiltonian, and the subsequent application of time and space Fourier transformations of the eigenvectors to determine the scattering intensities. This work demonstrates how edge anisotropy can be studied with INS of magnetic nanoparticles. Furthermore, it provides a framework for the study of surface spin waves in thin films and the surface of bulk systems.

Bibliography

[1] R.S. Fishman, J.A. Fernandez-Baca, and T. Rõõm. *Spin-Wave Theory and its Applications to Neutron Scattering and THz Spectroscopy*. IOP Concise Physics. Morgan & Claypool Publishers, 2018.

[2] Ian Aupiais, Pierre Hemme, Marc Allen, Alexis M. Scida, Xiao Lu, Christian Ricolleau, Yann Gallais, Alain Sacuto, Stanislaus S. Wong, Rogrio de Sousa, and Maximilien Cazayous. Impact of the surface phase transition on magnon and phonon excitations in bifeo3 nanoparticles. *Applied Physics Letters*, 116(17):172903, 2020.

[3] 1917-(editor.) Rado, George T. (George Tibor) and (editor.) Suhl, Harry. *Magnetism. Volume III, Spin arrangements and crystal structure, domains, and micromagnetics*. New York Academic Press, 1963. Includes bibliographical references and index.

[4] Nicola A. Spaldin. *Magnetic Materials: Fundamentals and Applications*. Cambridge University Press, 2 edition, 2010.

[5] R.C. O'Handley. *Modern Magnetic Materials: Principles and Applications*. Wiley, 1999.

[6] Sabah M. Abdelbasir and Ahmed Esmail Shalan. Intriguing properties and applications of functional magnetic materials. In Dipti Sahu, editor, *Functional Materials*, chapter 4. IntechOpen, Rijeka, 2019.

[7] S Karmakar, S Kumar, R Rinaldi, and G Maruccio. Nano-electronics and spintronics with nanoparticles. *Journal of Physics: Conference Series*, 292:012002, apr 2011.

[8] Xiaoming Li, Jianrong Wei, Katerina E. Aifantis, Yubo Fan, Qingling Feng, FuZhai Cui, and Fumio Watari. Current investigations into magnetic nanoparticles

for biomedical applications. *Journal of Biomedical Materials Research Part A*, 104(5):1285–1296, 2016.

[9] M.F. Hansen, F. Bdker, S. Mrup, K. Lefmann, K.N. Clausen, and P.-A. Lindgrd. Magnetic dynamics of fine particles studied by inelastic neutron scattering. *Journal of Magnetism and Magnetic Materials*, 221(1):10 – 25, 2000. Proceedings of the 3rd Euroconference on Magnetic Properties of Fine Particles and their Relevance to Materials Science.

[10] P. V. Hendriksen, S. Linderoth, and P.-A. Lindgård. Finite-size modifications of the magnetic properties of clusters. *Phys. Rev. B*, 48:7259–7273, Sep 1993.

[11] H. Puszkarski. Surface modes in magnetic thin films and in spin wave resonance. *IEEE Transactions on Magnetics*, 9(1):22–27, 1973.

[12] Henryk Puszkarski. Theory of surface states in spin wave resonance. *Progress in Surface Science*, 9(5):191 – 247, 1979.

[13] V. Veerakumar and R. E. Camley. Magnetostatic bulk and surface spin-wave focusing in antiferromagnetic thin films. *Phys. Rev. B*, 81:174432, May 2010.

[14] Marc Allen, Ian Aupiais, Maximilien Cazayous, and Rogério de Sousa. Size-dependent bistability in multiferroic nanoparticles. *Phys. Rev. Materials*, 3:084402, Aug 2019.

[15] Rogerio de Sousa and Joel E. Moore. Optical coupling to spin waves in the cycloidal multiferroic $BiFeo_3$. *Phys. Rev. B*, 77:012406, Jan 2008.

[16] E. Pavarini, E. Koch, F. Anders, and M. Jarrell. *Correlated Electrons: from Models to Materials*. Schriften des Forschungszentrums Jülich / Reihe Modeling and Simulation: Reihe Modeling and Simulation. Forschungszentrum Jülich, Zentralbibliothek, Verlag, 2012.

[17] Jerryman Gyamfi. *An Introduction to the Holstein-Primakoff Transformation, with Applications in Magnetic Resonance*. preprint, 06 2019.

[18] Kathryn L Krycka, James J Rhyne, Samuel D Oberdick, Ahmed M Abdelgawad, Julie A Borchers, Yumi Ijiri, Sara A Majetich, and Jeffrey W Lynn. Spin waves across three-dimensional, close-packed nanoparticles. *New Journal of Physics*, 20(12):123020, dec 2018.

[19] Ewen Smith and Geoffrey Dent. *Classical Theory of Rayleigh and Raman Scattering*, chapter 3, pages 31–48. John Wiley & Sons, Ltd, 2002.

[20] Tapan Chatterji. Chapter 1 - magnetic neutron scattering. In Tapan Chatterji, editor, *Neutron Scattering from Magnetic Materials*, pages 1 – 24. Elsevier Science, Amsterdam, 2006.

[21] Dino Fiorani, editor. *Surface Effects in Magnetic Nanoparticles*. Springer US, 1 edition, 2005.

[22] J.D. Jackson. *CLASSICAL ELECTRODYNAMICS, 3RD ED.* Wiley India Pvt. Limited, 2007.

[23] C. Kittel. *Quantum Theory of Solids*. Wiley, 1987.

[24] Louis Néel. Anisotropie magnétique superficielle et surstructures d'orientation. *J. Phys. Radium*, 15(4):225–239, 1954.

[25] C. P. Bean and J. D. Livingston. Superparamagnetism. *Journal of Applied Physics*, 30(4):S120–S129, 1959.

[26] Frandsen C. Hansen Mrup, S. and M. F. Beilstein. Uniform excitations in magnetic nanoparticles. *J. Nanotechnol.*, 1:4854, 2010.

[27] R.E Camley. Magnetization dynamics in thin films and multilayers. *Journal of Magnetism and Magnetic Materials*, 200(1):583 – 597, 1999.

[28] E.A. Denisova, S.V. Komogortsev, R.S. Iskhakov, L.A. Chekanova, A.D. Balaev, Yu.E. Kalinin, and A.V. Sitnikov. Magnetic anisotropy in multilayer nanogranular films. *Journal of Magnetism and Magnetic Materials*, 440:221 – 224, 2017. Selected papers from the sixth Euro-Asian Symposium Trends in Magnetism (EASTMAG-2016).

[29] J. C. S. Levy, Diep-The-Hung and O. Nagai. Effects of surface spin waves and surface anisotropy in magnetic thin films at finite temperatures. *physica status solidi (b)*, 93(1):351–361, 1979.

[30] Ryuichi Shindou, Jun-ichiro Ohe, Ryo Matsumoto, Shuichi Murakami, and Eiji Saitoh. Chiral spin-wave edge modes in dipolar magnetic thin films. *Phys. Rev. B*, 87:174402, May 2013.